

Flavour anomalies and the muon $g - 2$ from feebly interacting particles

Luc Darmé,^a Marco Fedele,^b Kamila Kowalska^c and Enrico Maria Sessolo^c

^a *INFN, Laboratori Nazionali di Frascati,
C.P. 13, 100044 Frascati, Italy*

^b *Institut für Theoretische Teilchenphysik, Karlsruhe Institute of Technology,
D-76131 Karlsruhe, Germany*

^c *National Centre for Nuclear Research,
ul. Pasteura 7, 02-093 Warsaw, Poland*

E-mail: luc.darme@lnf.infn.it, marco.fedele@kit.edu,
kamila.kowalska@ncbj.gov.pl, enrico.sessolo@ncbj.gov.pl

ABSTRACT: We perform a phenomenological analysis of simplified models of light, feebly interacting particles (FIPs) that can provide a combined explanation of the anomalies in $b \rightarrow sl^+l^-$ transitions at LHCb and the anomalous magnetic moment of the muon. Different scenarios are categorised according to the explicit momentum dependence of the FIP coupling to the $b-s$ and $\mu-\mu$ vector currents and they are subject to several constraints from flavour and precision physics. We show that viable combined solutions to the muon $g - 2$ and flavour anomalies exist with the exchange of a vector FIP with mass larger than 4 GeV. Interestingly, the LHC has the potential to probe this region of the parameter space by increasing the precision of the $Z \rightarrow 4\mu$ cross-section measurement. Conversely, we find that solutions based on the exchange of a lighter vector, in the $m_V < 1$ GeV range, are essentially excluded by a combination of $B \rightarrow K + \text{invisible}$ and W -decay precision bounds.

Contents

1	Introduction	1
2	EFT plus light degrees of freedom	3
3	Relation with the WET	4
3.1	Tree level	5
3.2	Loop-level	7
4	Flavour physics constraints	8
4.1	B -meson constraints	8
4.2	Lepton sector constraints	10
4.3	Muon anomalous magnetic moment	12
5	Numerical results	12
5.1	Fit to the $b \rightarrow s$ anomalies	13
5.2	Including all flavour constraints	16
6	Summary and conclusions	19
A	B-meson decays in the DEFT basis	21
A.1	$B \rightarrow K$ process	21
A.2	$B \rightarrow K^*$ process	22
A.3	$B_s \rightarrow \mu\mu$ and B_s -mixing processes	23

1 Introduction

Feebly interacting particles (FIPs) represent a very large and well-motivated category of new physics (NP) scenarios. Loosely defined as new light particles with mass below the electroweak symmetry-breaking (EWSB) scale and with a feeble interaction with Standard Model (SM) fields, FIPs encompass NP particles as diverse as the dark photon and axion-like particles. A particularly exciting possibility [1–8] is that one or more FIPs may be responsible for the anomalies in lepton-flavour universality violating (LFUV) observables recently confirmed in new data from LHCb and for the discrepancy between the measured value of the anomalous magnetic moment of the muon and its SM expectation.

The LHCb Collaboration recently released an updated measurement of the ratio $R_K = \text{BR}(B \rightarrow K\mu^+\mu^-)/\text{BR}(B \rightarrow Ke^+e^-)$, which included the full Run I + Run II data sets. The current value deviates from the SM prediction by more than 3σ [9]. Once the LFUV ratio $R_{K^*} = \text{BR}(B \rightarrow K^*\mu^+\mu^-)/\text{BR}(B \rightarrow K^*e^+e^-)$ [10, 11] and the branching ratios and angular observables of other decays mediated by $b \rightarrow sl^+l^-$ transitions [12–22] are

considered as well, a global picture emerges, pointing to the potential presence of NP interacting with the muons. These contributions are statistically favoured compared to the SM prediction alone, at the level of more than 5σ , see Refs. [23–36] for recent analyses.

Equally intriguing is the recent measurement of the anomalous magnetic moment of the muon by the E989 experiment at Fermilab [37]. The experimental collaboration reports a 3.3σ deviation from the value expected in the SM [38–57]. When the new measurement is statistically combined with the previous experimental determination, obtained a couple of decades ago at Brookhaven [58], one gets [37]

$$\delta(g - 2)_\mu = (2.51 \pm 0.59) \times 10^{-9}, \quad (1.1)$$

which yields a deviation from the SM data-driven prediction at the 4.2σ level.

If the LFUV anomalies and $\delta(g - 2)_\mu$ are due to the interactions of one or more FIPs in the MeV to GeV range, one expects the accompanying presence of new flavoured physics around the TeV scale (see, e.g., Ref. [8]). On the one hand, higher-dimensional FIP interactions, such as the ones characteristic of axion-like particle models, are simply effective field theories (EFTs) requiring an ultraviolet (UV) completion. On the other hand, even for renormalisable FIP interactions the presence of NP above the EWSB scale is often required, for instance to evade the strong bounds from neutrino trident production, which otherwise drastically constrains a solution to the $(g - 2)_\mu$ anomaly based on light states [59].

While a model-independent description of heavy physics in flavour-violating meson decay via the Weak Effective Theory (WET) has proved invaluable in identifying the specific operators associated with the anomalies emerging in a large set of observables, the WET fails to account properly for the possibility of one or more *extra* degrees of freedom that are light but hidden, as it is not by construction equipped to take into account the effects of momentum-dependent couplings, or the presence of possible resonances in the experimental energy bins. We thus consider in this work EFT operators more suited to the study of $b \rightarrow s$ and μ -related physics under the assumption that the unspecified heavy NP is accompanied by a light FIP [60, 61] (see also dark-matter motivated constructions, for instance Refs. [62–66]).

To this end, we construct a set of operators that parametrise the interactions of the FIP with Lorentz-invariant vector bilinears of the $b - s$ and $\mu - \mu$ current, in agreement with the measurement of the LFUV and $(g - 2)_\mu$ anomalies. They are characterised by increasing powers of the FIP momentum transferred in the low-energy process. We then perform a comprehensive analysis of the constraints that can be applied on the Wilson coefficients of these new operators. Constraints arise from several sources: direct measurements of the branching ratios for $B \rightarrow K + \text{invisible}$ and $B \rightarrow K^* \mu^+ \mu^-$ resonant decays, the measurements of $\text{BR}(B_s \rightarrow \mu^+ \mu^-)$ and B_s -mixing, and several precision measurements associated with the W - and Z -boson decay widths.

The purpose of our analysis is twofold. Firstly, we expand significantly on our previous study of a light “dark” $U(1)_D$ gauge boson solution to the $b - s$ anomalies with a q^2 -dependent coupling [8]. On the one hand, we add strong new constraints that were not considered previously in the literature (we compute numerically the best currently available

bounds on GeV-scale muonphilic particles from the recent ATLAS analysis of $Z \rightarrow 4\mu$ [67] and the limits based on the violation of flavour universality in W -boson decay [68]). On the other, we perform a global scan of two new simplified models with different momentum dependence of the couplings with respect to Ref. [8]. One of these models, incidentally, overlaps with the case considered in Ref. [2], for which we exclude the region of parameter space highlighted there and point to a slightly heavier preferred solution for the flavour and $(g-2)_\mu$ anomalies, with no fine tuning of the vector and axial-vector Z' couplings to the muon. The second and main goal of this work is to provide a concise and broad model-independent picture of the current phenomenological status of a light-FIP solution to the muon anomalies. In the process we will establish a “dictionary” allowing the reader to map easily the Wilson coefficients of a FIP-friendly EFT to the WET Wilson coefficients used in the publicly available numerical packages.

The paper is organised as follows. In Sec. 2 we introduce the operators better suited to describing FIP interactions in $b \rightarrow s$ and LFUV processes. In Sec. 3 we provide the correspondence with the WET basis usually employed in analyses of rare meson decays. The list of applied constraints is introduced in Sec. 4. The result of a global scan in the new operator basis are presented and discussed in Sec. 5, and we conclude in Sec. 6. In Appendix A we show the details required to perform a full calculation of processes involving the B meson in the basis introduced in Sec. 2.

2 EFT plus light degrees of freedom

We introduce in this section Dark EFT (DEFT) operators of the Lagrangian connecting a generic FIP to the (axial-)vector SM currents relevant for the LFUV and $(g-2)_\mu$ anomalies.

Spin-1 FIP We parametrise the exchange of a light vector V out of the left-handed $b-s$ current, in agreement with the results of the global fits, in terms of the following operators [5]:

$$\mathcal{Q}_4^{bsV} = (\bar{s}\gamma_\rho P_L b) V^\rho, \quad (2.1)$$

$$\mathcal{Q}_6^{bsV} = (\bar{s}\gamma_\rho P_L b) \partial_\sigma V^{\rho\sigma}, \quad (2.2)$$

where we have used the field strength tensor $V^{\rho\sigma} = \partial^\rho V^\sigma - \partial^\sigma V^\rho$.¹ We complete Eqs. (2.1), (2.2) with the corresponding interactions with the muon current,

$$\mathcal{Q}_4^{\mu\mu V} = (\bar{\mu}\gamma_\rho \mu) V^\rho, \quad \tilde{\mathcal{Q}}_4^{\mu\mu V} = (\bar{\mu}\gamma_\rho \gamma^5 \mu) V^\rho, \quad (2.3)$$

$$\mathcal{Q}_6^{\mu\mu V} = (\bar{\mu}\gamma_\rho \mu) \partial_\sigma V^{\rho\sigma}, \quad \tilde{\mathcal{Q}}_6^{\mu\mu V} = (\bar{\mu}\gamma_\rho \gamma^5 \mu) \partial_\sigma V^{\rho\sigma}. \quad (2.4)$$

Since we do not specify the origin of these interactions, Eqs. (2.1)-(2.4) will serve in describing the B -physics for all light vector states. These include, in particular, the GeV-scale top-philic particle in Ref. [69] and the renormalisable model introduced in Ref. [8].

¹We leave for future work the dimension 5 case, e.g., $\mathcal{Q}_5^{bsV} = (\bar{s}\sigma_{\rho\sigma} P_R b) V^{\rho\sigma}$. Since it couples the FIP to the tensor SM current it leads to a starkly different phenomenology.

Spin-0 FIP: the pNGB We consider next the case of a (pseudo-)scalar FIP, a , possibly a pseudo Nambu-Goldstone boson (pNGB). The standard derivative interaction term with the quark current reads

$$\mathcal{Q}_5^{bsa} = \frac{1}{2} \partial_\rho a (\bar{s} \gamma^\rho P_L b) , \quad (2.5)$$

and

$$\mathcal{Q}_5^{\mu\mu a} = \frac{1}{2} \partial_\rho a (\bar{\mu} \gamma^\rho \mu) , \quad \tilde{\mathcal{Q}}_5^{\mu\mu a} = \frac{1}{2} \partial_\rho a (\bar{\mu} \gamma^\rho \gamma^5 \mu) , \quad (2.6)$$

are the corresponding couplings to the muon current. These interactions are strongly constrained by flavour physics and, more importantly for our purposes, do not lead to the vector four-fermion operators $\mathcal{O}_9^{\mu(\prime)}$ and $\mathcal{O}_{10}^{\mu(\prime)}$ of the WET, which induce the solution to the LFUV anomalies preferred in the global scans. We therefore leave the study of these operators for future work.

FIPs as dark matter: spin 0, 1/2 When the light state is a stable new particle, which can play the role of dark matter, one needs to include operators with two FIP insertions at dimension 6. Using the dark current,

$$\mathcal{J}_D^\rho = \begin{cases} i(S^* \partial^\rho S - S \partial^\rho S^*) & (\text{scalar}, D = S) \\ \bar{\chi} \gamma^\rho \chi , & (\text{fermion}, D = \chi) \end{cases} \quad (2.7)$$

we can then define

$$\mathcal{Q}_6^{\mu\mu\chi\chi} = \mathcal{J}_\chi^\rho (\bar{\mu} \gamma_\rho \mu) , \quad \tilde{\mathcal{Q}}_6^{\mu\mu\chi\chi} = \mathcal{J}_\chi^\rho (\bar{\mu} \gamma_\rho \gamma^5 \mu) , \quad (2.8)$$

and

$$\mathcal{Q}_6^{bs\chi\chi} = \mathcal{J}_\chi^\rho (\bar{s} \gamma_\rho P_L b) , \quad (2.9)$$

and equivalent operators can be defined in the scalar case, with $\chi \rightarrow S$.

These effective interactions can be used to parametrise, for example, UV completions to the WET operators $\mathcal{O}_9^{\mu(\prime)}$, $\mathcal{O}_{10}^{\mu(\prime)}$ based on dark-matter induced box loops, in the case where the dark matter is relatively light. Note, however, that in such a minimal scenario the dark matter mass is expected to be large enough to evade strong limits from the direct decay $B \rightarrow K + \text{invisible}$ [8].

3 Relation with the WET

In order to quantify the effects of DEFT operators on the flavour observables, we first create a dictionary between the DEFT and the WET. The procedure is equivalent to considering an explicit momentum dependence of the WET Wilson coefficients, of the type explored, e.g., in Refs. [1, 3, 6, 8]. The specific Lorentz structure of the DEFT operators considered in this work allows us to draw the correspondence with the WET straightforwardly at the level of the spinor fields. We show in Appendix A that the results of this section agree with a full calculation of B -meson decays.

3.1 Tree level

Spin-0 FIP The critical ingredient in linking both theories is that we are interested in physical processes in which the muons are on-shell. Given two on-shell external muons of four-momenta k_1, k_2 , emerging from the exchange of a FIP of momentum $q = k_1 + k_2$, the equations of motions yield

$$q^\rho (\bar{\mu} \gamma_\rho \mu) = 0 \quad (3.1)$$

$$q^\rho (\bar{\mu} \gamma_\rho \gamma^5 \mu) = 2M_\mu (\bar{\mu} \gamma^5 \mu), \quad (3.2)$$

where M_μ is the muon mass. A direct consequence of the above equations is that the derivative scalar current introduced in Eqs. (2.5) and (2.6) will give rise to the standard pseudoscalar interactions $\mathcal{O}_P^{\mu(\prime)}$, and thus cannot generate the WET vector operators $\mathcal{O}_9^{\mu(\prime)}$ and $\mathcal{O}_{10}^{\mu(\prime)}$.

By repeating the argument for “on-shell” initial quarks with $q = p_b - p_s$, one obtains

$$(\bar{s} \gamma_\rho P_L b) q^\rho = M_s (\bar{s} P_L b) - M_b (\bar{s} P_R b), \quad (3.3)$$

where $M_{s(b)}$ is the strange (bottom) quark mass. The above equality is useful for deriving the correspondence between DEFT and WET in the remainder of this section.

Spin-1 FIP We write the vector FIP propagator in the form

$$\Pi^{\rho\sigma} = \frac{-i (g^{\rho\sigma} - q^\rho q^\sigma / m_V^2)}{\Pi}, \quad \text{with} \quad \Pi = q^2 - m_V^2 + i\Gamma_V \sqrt{q^2}, \quad (3.4)$$

where m_V and Γ_V indicate, respectively, the mass and total decay width of the light NP vector V^ρ . By considering the $b \rightarrow s\mu\mu$ process via a vector FIP exchange, we can derive the relation between the two effective theories. In the case, for example, of an interaction involving operators \mathcal{Q}_6^{bsV} and $\tilde{\mathcal{Q}}_4^{\mu\mu V}$ in Eqs. (2.2) and (2.3) one finds the amplitude

$$\begin{aligned} \mathcal{M} &= -\tilde{\mathcal{C}}_4^{\mu\mu V} \mathcal{C}_6^{bsV} / \Lambda^2 (\bar{s} \gamma_\rho P_L b) (q^2 g^{\sigma\rho} - q^\sigma q^\rho) \Pi_{\sigma\nu} (\bar{\mu} \gamma^\nu \gamma^5 \mu) \\ &= i \frac{\tilde{\mathcal{C}}_4^{\mu\mu V} \mathcal{C}_6^{bsV} / \Lambda^2}{\Pi} (\bar{s} \gamma_\rho P_L b) (q^2 \delta_\nu^\rho - q^\rho q_\nu) (\bar{\mu} \gamma^\nu \gamma^5 \mu). \end{aligned} \quad (3.5)$$

The above amplitude is expressed in terms of the UV cutoff, Λ , and the DEFT dimensionless coefficients \mathcal{C}_6^{bsV} , $\tilde{\mathcal{C}}_4^{\mu\mu V}$. This leads in turn to replacing the weak effective Hamiltonian for $b \rightarrow s\mu\mu$ with

$$\mathcal{H} \rightarrow -\frac{\tilde{\mathcal{C}}_4^{\mu\mu V} \mathcal{C}_6^{bsV}}{\Lambda^2 \Pi} \frac{4\pi}{\alpha_{\text{em}}} [q^2 \mathcal{O}_{10}^\mu + 2M_\mu (M_s \mathcal{O}_P^{\mu\prime} - M_b \mathcal{O}_P^\mu)], \quad (3.6)$$

where we have used the relation (3.3).

Following a similar procedure, we can connect to the WET all the operators introduced in Sec. 2a. The WET coefficients C_9^μ , C_{10}^μ , C_P^μ , $C_P^{\mu\prime}$, can then be expressed in terms of

DEFT coefficients. One gets,

$$C_9^\mu \rightarrow \frac{4\pi\mathcal{N}}{\alpha_{\text{em}}} \frac{(C_4^{bsV} + \frac{q^2}{\Lambda^2} C_6^{bsV})(C_4^{\mu\mu V} + \frac{q^2}{\Lambda^2} C_6^{\mu\mu V})}{q^2 - m_V^2 + i\Gamma_V \sqrt{q^2}}, \quad (3.7)$$

$$C_{10}^\mu \rightarrow \frac{4\pi\mathcal{N}}{\alpha_{\text{em}}} \frac{(C_4^{bsV} + \frac{q^2}{\Lambda^2} C_6^{bsV})(\tilde{C}_4^{\mu\mu V} + \frac{q^2}{\Lambda^2} \tilde{C}_6^{\mu\mu V})}{q^2 - m_V^2 + i\Gamma_V \sqrt{q^2}}, \quad (3.8)$$

$$C_P^\mu \rightarrow -\frac{4\pi\mathcal{N}}{\alpha_{\text{em}}} \frac{\frac{2M_\mu M_b}{m_V^2} C_4^{bsV} \left(\tilde{C}_4^{\mu\mu V} + \frac{m_V^2}{\Lambda^2} \tilde{C}_6^{\mu\mu V} \right) + \frac{2M_\mu M_b}{\Lambda^2} C_6^{bsV} \left(\tilde{C}_4^{\mu\mu V} + \frac{q^2}{\Lambda^2} \tilde{C}_6^{\mu\mu V} \right)}{q^2 - m_V^2 + i\Gamma_V \sqrt{q^2}}, \quad (3.9)$$

$$C_P^\mu \rightarrow \frac{4\pi\mathcal{N}}{\alpha_{\text{em}}} \frac{\frac{2M_\mu M_s}{m_V^2} C_4^{bsV} \left(\tilde{C}_4^{\mu\mu V} + \frac{m_V^2}{\Lambda^2} \tilde{C}_6^{\mu\mu V} \right) + \frac{2M_\mu M_s}{\Lambda^2} C_6^{bsV} \left(\tilde{C}_4^{\mu\mu V} + \frac{q^2}{\Lambda^2} \tilde{C}_6^{\mu\mu V} \right)}{q^2 - m_V^2 + i\Gamma_V \sqrt{q^2}}, \quad (3.10)$$

where $\mathcal{N}^{-1} = (4G_F/\sqrt{2}) V_{tb}V_{ts}^*$.

An explicit UV example We conclude this subsection by matching the DEFT operators to an example of renormalisable UV-complete model in the case of a vector FIP. We focus on the flavour-violating coupling to b and s .

Let us consider the SM extended by a “dark” $U(1)_D$ gauge group, whose gauge boson is a light V . Let us then introduce a scalar field ϕ and a multiplet χ of vector-like fermions of mass m_χ whose charges with respect to $SU(3)_c \times SU(2)_L \times U(1)_Y \times U(1)_D$ are given by

$$\phi : (\mathbf{1}, \mathbf{1}, 0, Q_\phi) \quad \chi : (\mathbf{3}, \mathbf{2}, 1/6, Q_\chi). \quad (3.11)$$

When $Q_\phi = Q_\chi$ the fields in Eq. (3.11) admit Yukawa interactions with the SM quark doublets $Q_i = (P_L u_i, P_L d_i)^T$ (of generation $i = 2, 3$) of the type

$$\mathcal{L} \supset Y_Q^i \phi \bar{\chi} Q_i + \text{H.c.} \quad (3.12)$$

Depending on whether or not the field ϕ acquires a vacuum expectation value (vev) different DEFT operators of the $b - s$ current are generated at the leading order from the coupling in Eq. (3.12). If ϕ develops a vev, v_ϕ , the effective coupling of V to $b - s$, which is generated via the mixing of the SM and NP quarks, does not carry q^2 dependence and thus gives rise to the operator Q_4^{bsV} . One gets

$$C_4^{bsV} = g_D Q_\phi \frac{Y_Q^{s*} Y_Q^b v_\phi^2}{2m_\chi^2 + \left(|Y_Q^s|^2 + |Y_Q^b|^2 \right) v_\phi^2}, \quad (3.13)$$

where g_D is the dark gauge coupling. The phenomenology of the light gauge boson V in relation to $R_{K^{(*)}}$ was analysed, e.g., in Ref. [2].

If, on the other hand, the scalar ϕ does not develop a vev and $U(1)_D$ is broken by other means unspecified here, the coupling of V to the $b - s$ current is generated via a penguin

diagram constructed out of a $\phi\chi$ loop. Terms presenting an explicit q^2 dependence give rise to the operator \mathcal{Q}_6^{bsV} . Its Wilson coefficient reads

$$\frac{\mathcal{C}_6^{bsV}}{\Lambda^2} = \frac{g_D Q_\phi Y_Q^{s*} Y_Q^b}{16\pi^2 m_\chi^2} \mathcal{F}\left(\frac{m_\phi^2}{m_\chi^2}\right), \quad (3.14)$$

where m_ϕ is the mass of the scalar field and the loop function is [70]

$$\mathcal{F}(x) = \frac{3 - 3x + (1 + 2x) \ln x}{6(x - 1)^2}. \quad (3.15)$$

When $m_\phi \ll m_\chi \approx \Lambda$, \mathcal{Q}_6^{bsV} becomes the dominant operator emerging from the $\phi\chi$ loop, thanks to the logarithmic enhancement in Eq. (3.15). The phenomenology of this “split” dark sector was analysed in Ref. [8] and q^2 -dependent operators were considered also in Refs. [1, 3, 6].

Analogous to this is the case where fermion and scalar multiplet charges are swapped in Eq. (3.11) [8], and UV constructions along similar lines can be considered to generate the DEFT operators involving the muon current in Eqs. (2.3), (2.4).

Note that the DEFT coefficients \mathcal{C}_4^{bsV} , \mathcal{C}_6^{bsV} – similarly to $C_{9(10)}^\mu$ in the WET – do not run at the leading order in QCD, since their colour part is simply a vector current [71].²

3.2 Loop-level

In the case of FIPs as dark matter particles one typically obtains the Wilson coefficients of the WET from “candy” diagrams constructed out of the operators in Eqs. (2.8), (2.9). By making use of a simple cut-off regularisation, one can derive at one loop the Wilson coefficient C_9^μ from a fermion FIP insertion,

$$C_9^{\mu(\text{ferm.})} = -\frac{\mathcal{N} \mathcal{C}_6^{bs\chi\chi} \mathcal{C}_6^{\mu\mu\chi\chi}}{2\pi \alpha_{\text{em}} \Lambda^2}. \quad (3.16)$$

A scalar FIP leads to

$$C_9^{\mu(\text{scal.})} = -\frac{\mathcal{N} \mathcal{C}_6^{bsSS} \mathcal{C}_6^{\mu\mu SS}}{16\pi \alpha_{\text{em}} \Lambda^2}. \quad (3.17)$$

Note that the only other scale that enters directly the WET coefficients in Eqs. (3.16) and (3.17), apart from the EWSB scale, is the Λ^2 suppression. The exact value of the coefficients will thus depend on the specific nature of the heavy UV completion and, as a direct consequence, the light dark matter mass will have no impact on the flavour anomalies as long as its couplings to the $b - s$ and $\mu - \mu$ current are mediated by states that can be integrated out of the low-energy theory.

²Conversely, a DEFT coefficient corresponding to a tensor operator of the type $\mathcal{Q}_5^{bsV} = (\bar{s}\sigma_{\rho\sigma} P_R b) V^{\rho\sigma}$, which can also be generated at the loop level by the UV completion, has to be renormalised before being confronted with the low-energy constraints. We leave the treatment of this and other less straightforward cases to future work.

4 Flavour physics constraints

Global scans combining the constraints from the LFUV ratios R_K and R_{K^*} with the full set of $b \rightarrow sl^+l^-$ branching ratios and angular observables convincingly show the emergence of NP effects in the WET Wilson coefficient C_9^μ , which can be taken alone or in combinations with others. When parametrising the global fit with one NP degree of freedom, the expected size of the Wilson coefficient is $-1.1 \lesssim C_9^\mu \lesssim -0.5$ at 2σ in the single-operator case, or $-0.6 \lesssim C_9^\mu = -C_{10}^\mu \lesssim -0.3$ in a linear combination of \mathcal{O}_9^μ and \mathcal{O}_{10}^μ [23–36].

As we have shown in Sec. 3.1, the insertion of a spin-0 FIP cannot generate the WET operator \mathcal{O}_9^μ (or \mathcal{O}_{10}^μ). At the same time, Eqs. (3.16), (3.17) show that the numerical value of C_9^μ is quite insensitive to the presence of light dark matter-like spin-1/2 and/or spin-0 states with dimension 6 interactions. We can thus choose to limit our attention to the only case in which the presence of a light FIP has direct impact on the $b \rightarrow sl^+l^-$ global fit: the vector FIP.

The constraints on C_9^μ and other WET coefficients derived from the flavour anomalies lead in this case to a typical order-of-magnitude estimate for the DEFT couplings, obtained from a spin-1 FIP exchange in $b \rightarrow s\mu\mu$, see Eqs. (3.7), (3.8). One gets

$$\mathcal{C}_{4+\delta_1}^{bsV} \mathcal{C}_{4+\delta_2}^{\mu\mu V} \left(\frac{q}{\Lambda}\right)^{\delta_1+\delta_2} \approx 10^{-9}, \quad (4.1)$$

where $4 + \delta_{1,2}$ indicates the dimension of the corresponding operator, and q is the typical energy exchange captured in the experimental bin. For example, the biproduct of operators $\mathcal{Q}_6^{bsV} \times \mathcal{Q}_4^{\mu\mu V}$ develops q^2 dependence in the couplings, while this is not the case for a combination of operators of dimension 4.

The presence of a new light vector particle in the spectrum has far reaching consequence for a variety of SM processes. As is discussed in the literature (see, e.g., Refs. [72–74]), at FIP masses far below the typical energy scale E of a given SM process, the phenomenology is dominated by the FIP longitudinal polarisation V_L as $V_\mu \rightarrow \partial_\mu V_L/m_V$. While this mode cancels out for dimension-6 interactions like Eqs. (2.2) and (2.4), it dominates for the dimension-4 cases, Eqs. (2.1) and (2.3), as they do not correspond to conserved SM fermionic currents. More precisely, the interactions presented in Eq. (2.1) and Eq. (2.3) lead to tree-level flavour violation, weak-isospin violation (since no coupling to neutrinos where included) and an axial-coupling interaction to the SM fermions. We examine in this section the most relevant of the corresponding limits.

4.1 B -meson constraints

We first consider the constraints from B -meson physics.

$B_s \rightarrow \mu\mu$ Based on a physical process related to the one generating $B \rightarrow K^{(*)}\mu^+\mu^-$ transitions, $\text{BR}(B_s \rightarrow \mu^+\mu^-)$ can provide a strong constraint on axial muon interactions. After performing a statistical combination of the full LHCb Run 2 data with the global average of Ref. [75], Ref. [33] finds

$$\text{BR}(B_s \rightarrow \mu^+\mu^-)_{\text{exp. ave.}} = (2.93 \pm 0.35) \times 10^{-9}. \quad (4.2)$$

The ratio R_{B_s} between Eq. (4.2) and the SM prediction, $\text{BR}(B_s \rightarrow \mu^+ \mu^-)_{\text{SM}} = (3.67 \pm 0.15) \times 10^{-9}$ [76], can be parametrised in terms of the DEFT. For a vector FIP, exchanged between the currents \mathcal{Q}_4^{bsV} and $\tilde{\mathcal{Q}}_4^{\mu\mu V}$, we replace the WET Wilson coefficients C_{10}^μ , C_P^μ , $C_P^{\mu'}$ like in Eqs. (3.8)-(3.10). Substituting into standard expressions [77] one gets

$$\begin{aligned} R_{B_s} &= \frac{\text{BR}(B_s \rightarrow \mu^+ \mu^-)_{\text{exp.}}}{\text{BR}(B_s \rightarrow \mu^+ \mu^-)_{\text{SM}}} - 1 \\ &\simeq -\frac{8\pi\mathcal{N} C_4^{bsV} \tilde{\mathcal{C}}_4^{\mu\mu V}}{\alpha_{\text{em}} C_{10}^{\text{SM}} m_V^2} \frac{(m_V^2 - M_{B_s}^2)^2}{(m_V^2 - M_{B_s}^2)^2 + M_{B_s}^2 \Gamma_V^2}, \end{aligned} \quad (4.3)$$

where $C_{10}^{\text{SM}} = -4.31$ and we have taken the small coupling limit. Equation (4.2) excludes the SM prediction at 2σ , we thus choose to impose the bound at 3σ to avoid cutting out all the points with a zero or extremely small NP contribution. On the other hand, we observe that Eq. (4.3) is negative if $C_4^{bsV} \tilde{\mathcal{C}}_4^{\mu\mu V} > 0$, which implies that NP contributions can potentially bring R_{B_s} closer to the measured value. As we shall see in the next section, this sign choice is indeed preferred for m_V larger than a few GeV. Conversely, we shall see that in the low mass regime ($m_V \lesssim 1 \text{ GeV}$) one gets $C_4^{bsV} \tilde{\mathcal{C}}_4^{\mu\mu V} < 0$, which produces a strong upper bound at 3σ :

$$\left| C_4^{bsV} \tilde{\mathcal{C}}_4^{\mu\mu V} \right| \lesssim 1.5 \cdot 10^{-10} \left(\frac{m_V}{1 \text{ GeV}} \right)^2. \quad (4.4)$$

Fundamentally different are the cases of the pairs of operators \mathcal{Q}_6^{bsV} , $\tilde{\mathcal{Q}}_4^{\mu\mu V}$ and \mathcal{Q}_6^{bsV} , $\tilde{\mathcal{Q}}_6^{\mu\mu V}$ for which we find that the NP contribution to $B_s \rightarrow \mu\mu$ vanishes exactly, $R_{B_s} = 0$, since the term contributing to the axial component is cancelled by the one feeding into the pseudoscalar current. Interestingly, this implies that increasing the sensitivity of the measurement of $\text{BR}(B_s \rightarrow \mu^+ \mu^-)$ may provide a handle to distinguish scenarios characterised by operators of different dimension.

B_s -mixing $B_s - \bar{B}_s$ transitions can constrain the operators introduced in Sec. 2. We use [68]

$$R_{\Delta M_s} = \frac{\Delta M_s^{\text{exp.}}}{\Delta M_s^{\text{SM}}} - 1 = -0.09 \pm 0.08 \quad (4.5)$$

to impose a bound on the DEFT Wilson coefficients of the $b-s$ current via the dictionary between the DEFT and the WET shown in Eqs. (A.30)-(A.34) of Appendix A.3.

Similarly to the $B_s \rightarrow \mu\mu$ case, the severity of the bound strongly depends on which DEFT operator is generated in the UV completion yielding the $b-s$ coupling. The operator \mathcal{Q}_4^{bsV} leads to an m_V^2 -rescaled modification of the WET Wilson coefficients C_2 , \tilde{C}_2 , and C_4 . We obtain, in the small coupling approximation,

$$R_{\Delta M_s} \simeq -\frac{(C_4^{bsV})^2}{C_1^{\text{SM}}(\mu_b) m_V^2} \frac{(M_{B_s}^2 - m_V^2)(m_V^2 + R_2 M_b^2)}{(m_V^2 - M_{B_s}^2)^2 + M_{B_s}^2 \Gamma_V^2}, \quad (4.6)$$

where $C_1^{\text{SM}}(\mu_b) = 7.2 \times 10^{-11} \text{ GeV}^{-2}$ and $R_2(\mu_b) \simeq -0.96$ is the ratio of the matrix elements $\langle \bar{B}_s | \mathcal{O}_2(\mu_b) | B_s \rangle / \langle \bar{B}_s | \mathcal{O}_1(\mu_b) | B_s \rangle$ (see, e.g., Ref. [78] for an updated value), all computed at the b -quark mass scale, μ_b . As was mentioned above, we have not run the SM Wilson

coefficients since we compare operators directly at the B_s scale. By combining Eq. (4.6) and Eq. (4.5) one gets a strong constraint in the $m_V \ll 1$ GeV range: $|\mathcal{C}_4^{bsV}| \lesssim 2.5 \cdot 10^{-6} m_V/\text{GeV}$. Conversely, with UV interactions giving rise to the operator \mathcal{Q}_6^{bsV} , Eq. (4.5) becomes

$$R_{\Delta M_s} \simeq -\frac{M_{B_s}^2 (\mathcal{C}_6^{bsV})^2 (M_{B_s}^2 - m_V^2)(M_{B_s}^2 + R_2 M_b^2)}{\Lambda^4 C_1^{\text{SM}}(\mu_b) (m_V^2 - M_{B_s}^2)^2 + M_{B_s}^2 \Gamma_V^2}. \quad (4.7)$$

One obtains $|\mathcal{C}_6^{bsV}| M_{B_s}^2/\Lambda^2 \lesssim 5 \times 10^{-5}$ in the low m_V region.

$B \rightarrow K^{(*)} X$ Strong limits arise from the direct measurement of the branching ratios of the V , both in the case of a visible resonance and that of an invisible decay. Resonant decays to visible particles are subject to extremely strong constraints from LHCb in the m_V range between $2M_\mu$ and $M_B - M_{K^*}$ [79]. We apply this bound following the numerical recast described in detail in Ref. [8].

To impose bounds on the invisible decay width we use a combination of BaBar results [80, 81].³ The adopted numerical procedure is described in detail in Appendix A of Ref. [8]. Assuming a large Γ_V to invisible final states in the $m_V \ll 1$ GeV range, the bin-dependent bounds on $\text{BR}(B \rightarrow K + \text{inv.})$ induce a strong constraint on the coupling to the hadronic current. In the dimension 4 case we get $|\mathcal{C}_4^{bsV}| \lesssim 10^{-8} m_V/\text{GeV}$, whereas for the operator of dimension 6 we get $|\mathcal{C}_6^{bsV}/\Lambda^2| \lesssim 5 \cdot 10^{-9} \text{GeV}^{-2}$.

4.2 Lepton sector constraints

The second set of constraints relies instead on probing the FIP interactions with muons, the most relevant of which arise from precision measurements of the W and Z decays.

W and Z decays In order to further probe the parameter space, we perform a simple recast of the result from the ATLAS Collaboration [67] on $pp \rightarrow \ell\ell\ell\ell$ (referred to as the $Z \rightarrow 4\mu$ search hereafter) in the Z -boson mass window. We implement our effective Lagrangian via FEYNRULES/UFO [83–85] files, then generate hadron-level events $pp \rightarrow \mu\mu\mu\mu$ within the MADGRAPH5_aMC@NLO platform [86], including the selection cuts from Ref. [67].⁴ Our simple simulation chain leads to a SM fiducial cross-section of 22 fb, in good agreement with the predicted SM result from Ref. [67], 21.2 ± 1.3 fb. We therefore use the final measured result of 22.1 ± 1.3 fb to constrain our parameter space. Note that interference with the SM plays an important role in the final cross-section computation.⁵

When the FIP is produced on-shell, an additional constraint on its couplings to muons arises from precision measurements of Drell-Yan dimuon production, as was shown in Ref. [88]. We find, however, that this limit is of the same order as the $Z \rightarrow 4\mu$ ATLAS bound, or even subdominant, for the mass range $m_V = 1 - 5$ GeV in which it was quoted.

³First results from a similar Belle-II search [82] agree with Refs. [80, 81].

⁴We include the following cuts: four-leptons invariant mass in the range 60 – 100 GeV, opposite-sign dilepton pair invariant mass larger than 5 GeV, $p_T > 20$ GeV for the leading lepton and $p_T > 10$ GeV for the sub-leading lepton, and an angular separation cut as detailed in Ref. [67].

⁵A somehow similar search was performed by the CMS Collaboration [87] with focuses on $L_\mu - L_\tau$ models. It yields constraints similar to the included ATLAS analysis.

Note that the on-shell V production, $Z \rightarrow \mu\mu V$, participates directly in the $Z \rightarrow 4\mu$ search and introduces a dependence of this limit to the invisible decay width of V .

In the low m_V regime, the presence of the massive vector FIP longitudinal mode leads to a E^2/m_V^2 enhancement of various SM decay widths. In particular, in the limit $M_\mu, m_V \ll M_Z, M_W$ we find

$$\Gamma(W \rightarrow \nu\mu V) \simeq \frac{\left(\mathcal{C}_4^{\mu\mu V} - \tilde{\mathcal{C}}_4^{\mu\mu V}\right)^2 G_F M_W^5}{512\sqrt{2}\pi^3 m_V^2}, \quad (4.8)$$

and

$$\frac{\Gamma(W \rightarrow \nu\mu) + \Gamma(W \rightarrow \nu\mu V)}{\Gamma(W \rightarrow \nu e)} \simeq 1 + \frac{\Gamma(W \rightarrow \nu\mu V)}{\text{BR}_{W \rightarrow e\nu} \Gamma_W}. \quad (4.9)$$

We then use the world experimental average on the ratio $\Gamma(W \rightarrow \nu\mu)/\Gamma(W \rightarrow \nu e)$, 0.996 ± 0.008 [68], to derive the 2σ limit

$$\left|\mathcal{C}_4^{\mu\mu V} - \tilde{\mathcal{C}}_4^{\mu\mu V}\right| \leq 0.004 \left(\frac{m_V}{100 \text{ MeV}}\right), \quad (4.10)$$

which holds as long as V decays mostly invisibly. A more conservative limit (which would also apply in presence of electron couplings) is simply to require Eq. (4.8) to be smaller than the total uncertainty on the measured W width. Using $\Gamma_W = 2.085 \pm 0.042 \text{ GeV}$ from Ref. [68], one obtains the 2σ bound

$$\left|\mathcal{C}_4^{\mu\mu V} - \tilde{\mathcal{C}}_4^{\mu\mu V}\right| < 0.022 \left(\frac{m_V}{100 \text{ MeV}}\right), \quad (4.11)$$

which agrees with Ref. [89].

Resonance search in B-factories The BaBar Collaboration has searched for the process $e^+e^- \rightarrow \mu^+\mu^-V$, $V \rightarrow \mu^+\mu^-$, when the FIP is assumed to have a small width and a mass up to around 10 GeV [90]. In the relevant mass region, our model requires in any case a large invisible width to escape resonant $B \rightarrow K^*\mu\mu$ searches, so that this constraint is subdominant. The Belle-II Collaboration recently provided a bound on the final-state radiation process $e^+e^- \rightarrow \mu^+\mu^-V$, $V \rightarrow \text{invisible}$, based on 0.28 fb^{-1} of data from the 2018 run [91]. While the current limit can hardly compete with other bounds the 2019 run has stored $\sim 10 \text{ fb}^{-1}$ of data so that the search is expected to become rapidly relevant in the near future.

Coupling to electrons We choose not to consider in this work explicit interactions of the FIP with electrons. Nevertheless, a coupling to electrons is generated via the vector kinetic mixing when at least one of the DEFT operators is at dimension 4 [92]. Thus, even below the di-muon threshold, we expect V to decay visibly into e^+e^- in the absence of an invisible decay channel. Constraints on a light vector FIP coupled to electrons were discussed, e.g., in Refs. [3, 5]. In particular, resonance searches at low q^2 in LHCb [13, 93] exclude the parameter space relevant for the $b \rightarrow s$ anomalies, thus requiring the V to decay mostly invisibly (in which case the constraints on $B \rightarrow K + \text{inv.}$ described above apply).⁶

⁶LHCb low-resonance searches extend down to $\sim 20 \text{ MeV}$. A very light electron-philic FIP is therefore not constrained by this approach. However, stringent limits on long-lived dark photons then apply, with the parameter space almost completely covered [94].

4.3 Muon anomalous magnetic moment

If the flavour anomalies are explained by a vector FIP exchange, the same FIP can potentially contribute to the anomalous magnetic moment of the muon. The recent confirmation at Fermilab [37] of a 3.3σ discrepancy between the observed value of $(g-2)_\mu$ and the SM renders this possibility all the more enticing and timely.

The computation of $(g-2)_\mu$ can be enhanced at the 1-loop level if the vector FIP V interacts with the muon current via $\mathcal{Q}_4^{\mu\mu V}$ and $\tilde{\mathcal{Q}}_4^{\mu\mu V}$. One gets [95, 96]

$$\delta(g-2)_\mu = \frac{1}{8\pi^2} \frac{M_\mu^2}{m_V^2} \left[(\mathcal{C}_4^{\mu\mu V})^2 \mathcal{F}(x_\mu) + (\tilde{\mathcal{C}}_4^{\mu\mu V})^2 \tilde{\mathcal{F}}(x_\mu) \right], \quad (4.12)$$

where $x_\mu = M_\mu/m_V$ and the loop functions read

$$\mathcal{F}(x) = \int_0^1 dz \frac{2z^2(1-z)}{x^2z + (1-z)(1-x^2z)}, \quad (4.13)$$

$$\tilde{\mathcal{F}}(x) = \int_0^1 dz \frac{[2z(1-z)(z-4) - 4x^2z^3]}{x^2z + (1-z)(1-x^2z)}. \quad (4.14)$$

Conversely, no significant enhancement is obtained if the coupling of the FIP to the muon proceeds through the operators $\mathcal{Q}_6^{\mu\mu V}$ and $\tilde{\mathcal{Q}}_6^{\mu\mu V}$. In those cases the value of $(g-2)_\mu$ is suppressed by the UV cut-off Λ yielding, for example,

$$\delta(g-2)_\mu = \frac{(\mathcal{C}_6^{\mu\mu V})^2 M_\mu^2}{12\pi^2\Lambda^2}, \quad (4.15)$$

in the case of $\mathcal{Q}_6^{\mu\mu V}$ and a similar expression for $\tilde{\mathcal{Q}}_6^{\mu\mu V}$. Its exact numerical value depends entirely on the specifics of the UV completion.

As we have described in Sec. 4.1, the viable range of the DEFT coefficients \mathcal{C}_4^{bsV} , \mathcal{C}_6^{bsV} , corresponding to the operators of the $b-s$ current, is bounded by the constraints from B_s -mixing and $B \rightarrow K^{(*)}X$ searches. As a direct consequence, for some points in the numerical scan the typical values of $\mathcal{C}_4^{\mu\mu V}$ required for a reasonable agreement with the flavour anomalies is very large, leading to a deviation in $\delta(g-2)_\mu$ widely exceeding the measured value. A cancellation with the contribution from the axial-vector coupling $\tilde{\mathcal{C}}_4^{\mu\mu V}$ may therefore be necessary [2]. In particular, as we will show in the next section, such cancellation is always required for light m_V whereas it is not needed for a GeV-scale FIP. Note that including the axial-vector contribution can trigger the bounds from $B_s \rightarrow \mu\mu$, also discussed in Sec. 4.1, which are particularly strong in the $m_V \ll 1$ GeV range.

5 Numerical results

In the rest of this work we will consider somehow arbitrarily FIP masses up to 20 GeV, so that $m_V^2/\Lambda_{\text{EW}}^2 \ll 1$. While there is no specific upper bound on the mass of the vector FIP from the constraints listed in the previous section, we also do not include in our simplified models the interactions between V and the electroweak sector. We leave the complete study of the “transitional” regime for larger masses, up to the electroweak scale Λ_{EW} , for future work.

5.1 Fit to the $b \rightarrow s$ anomalies

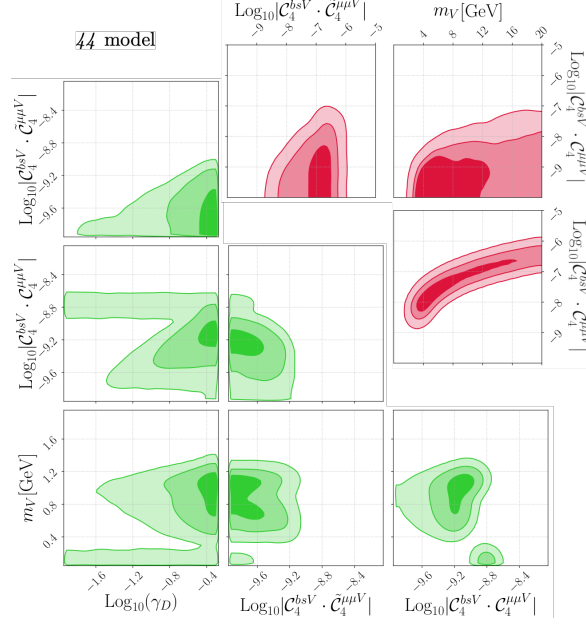
We perform a multidimensional fit to the $b \rightarrow s$ anomalies, including in particular the LFUV ratios R_K [9] and R_{K^*} [10], the most updated $B \rightarrow K^* \mu^+ \mu^-$ angular-observable data [21], and the finely binned results for the $B \rightarrow K \mu^+ \mu^-$ and $B \rightarrow K^* \mu^+ \mu^-$ branching ratios [12, 17]. We scan over the following free parameters: m_V , $\gamma_V \equiv \Gamma_V/m_V$, $\mathcal{C}_{4,6}^{bsV}$, $\mathcal{C}_{4,6}^{\mu\mu V}$, and $\tilde{\mathcal{C}}_{4,6}^{\mu\mu V}$. The vector mass m_V , expressed in GeV, is flatly distributed either in the $[0.01, 2]$ range, or in the $[2, 20]$ one. For the ratio between the V width and its mass, γ_V , we employ a logarithmically-flat prior in the range $[10^{-3}, 0.5]$. All the absolute values of the DEFT coefficients have a logarithmically-flat distributed prior in the range $[10^{-10}, 1]$. Since the observables included in these fits depend only on the products $\mathcal{C}_i^{bsV} \cdot \mathcal{C}_j^{\mu\mu V}$ and $\mathcal{C}_i^{bsV} \cdot \tilde{\mathcal{C}}_j^{\mu\mu V}$, but not on the single coefficients, the fit results presented in this subsection are given in terms of DEFT biproducts rather than as a function of individual coefficients.

As was described in detail in Ref. [8], we perform separate fits depending on whether m_V lies above or below 2 GeV. In fact, in order to obtain an adequate fit, one has to require that the product $\mathcal{C}_i^{bsV} \cdot \mathcal{C}_j^{\mu\mu V}$ ($\mathcal{C}_i^{bsV} \cdot \tilde{\mathcal{C}}_j^{\mu\mu V}$) assumes a different sign in each of these two regions. We note that this leads to a negative (positive) C_9^μ (C_{10}^μ), in agreement with the global WET fits. Following Ref. [8], we refer to these distinct cases as the *high-mass* fit and the *low-mass* fit.

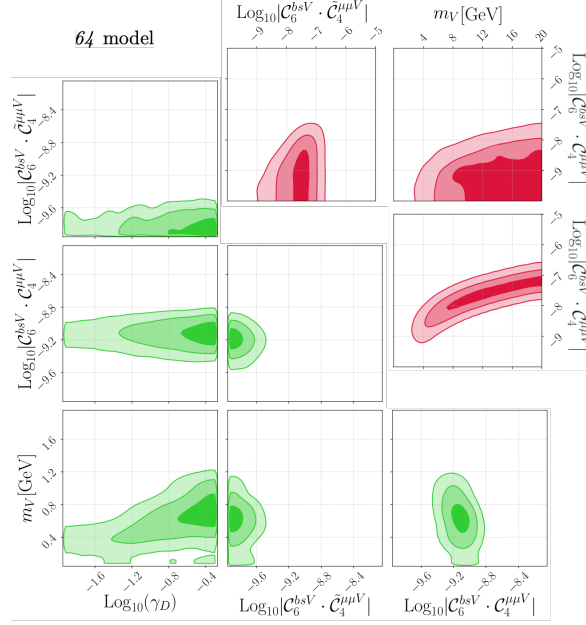
Due to the q^2 dependence of Eqs. (3.7)-(3.10), it is not possible to refer explicitly to the results of the global WET fits that can be found in the literature. One needs instead to confront the DEFT parameter space directly with the experimental data. In order to do so, we employ a custom version of the `HEPfit` package [97], performing a Markov Chain Monte Carlo analysis by means of the Bayesian Analysis Toolkit (BAT) [98].

We present in Fig. 1(a) the results of the fit in the case of DEFT operators of dimension 4 in both the $b - s$ and $\mu - \mu$ currents (we dub this as the *44 model* hereafter). The plots in red are relative to the high-mass fit, where $\mathcal{C}_4^{bsV} \cdot \mathcal{C}_4^{\mu\mu V}$ is required to be negative, the plots in green are relative to the low-mass one, where $\mathcal{C}_4^{bsV} \cdot \mathcal{C}_4^{\mu\mu V}$ is required to be positive, and the contours correspond to the smallest regions of 68%, 95%, 99.7% probability. In particular, in Fig. 1(a) we are showing the marginalised 2-dimensional posterior probability density function (2D pdf) in planes of the vector mass m_V , width-to-mass ratio γ_V , and the products of DEFT coefficients $\mathcal{C}_4^{bsV} \cdot \mathcal{C}_4^{\mu\mu V}$ and $\mathcal{C}_4^{bsV} \cdot \tilde{\mathcal{C}}_4^{\mu\mu V}$. In accordance with the respective priors, the posterior pdf's for the width and the coefficients are reported in logarithmic scale. The 2D pdf's involving γ_V are only shown for the low-mass fit since they are flatly distributed in the high-mass case and hence not particularly informative.

In the high-mass region of Fig. 1(a) (in red) one can observe a strong correlation between the vector mass m_V and the coupling product $\mathcal{C}_4^{bsV} \cdot \mathcal{C}_4^{\mu\mu V}$, responsible for the NP contributions to C_9^μ , cf. Eq. (3.7). The coupling biproduct can range from $\sim 10^{-8}$ (corresponding to $m_V \approx 4$ GeV) up to $\sim 10^{-6}$ at the 2σ level, if m_V grows as well. From the correlation between $\mathcal{C}_4^{bsV} \cdot \mathcal{C}_4^{\mu\mu V}$ and $\mathcal{C}_4^{bsV} \cdot \tilde{\mathcal{C}}_4^{\mu\mu V}$ it is also possible to observe that the latter can grow from negligible values up to the size of the former (at the 3σ level) but never get larger. This is consistent with the results of global WET fits [23–36], where NP contributions to C_{10}^μ – which, as Eq. (3.8) shows, in the DEFT arise precisely from



(a)



(b)

Figure 1: (a) Inference of model parameters from a fit to $b \rightarrow s$ anomalous data for the DEFT operators of dimension 4 in both the $b-s$ and $\mu-\mu$ currents (44 model). (b) Same for DEFT operator of dimension 6 in the $b-s$ current and dimension 4 in $\mu-\mu$ (64 model). The plots in red are relative to the high-mass fits (see main text) while the ones in green are relative to the low-mass ones, with the contours corresponding to the smallest regions of 68%, 95%, 99.7% probability. We refer to the main text for the sign of the couplings. Note that in (b) the coupling C_6^{bsV} is reported in units of GeV^{-2} .

$\mathcal{C}_4^{bsV} \cdot \tilde{\mathcal{C}}_4^{\mu\mu V}$ – are, if non-vanishing, usually smaller in size than the ones to C_9^μ .⁷ Note that the solution identified in Ref. [2], corresponding to a mediator with mass $m_V \approx 2.5$ GeV is disfavoured in our study. This is due to primarily two reasons. On the one hand, the set of observables in Ref. [2] included only the LFUV ratios and P'_5 , neglecting other measurements, e.g., the branching ratio $\text{BR}(B \rightarrow K^* \mu^+ \mu^-)$ [17], which generate large chi-squared values for $m_V \approx 2.5$ GeV. On the other hand, the recently updated values for the angular analysis of $B \rightarrow K^* \mu^+ \mu^-$, and hence for P'_5 , also push the favoured values for m_V above the region highlighted in Ref. [2].

In the low-mass region (in green) $\mathcal{C}_4^{bsV} \cdot \mathcal{C}_4^{\mu\mu V}$ ranges between $10^{-10.0} - 10^{-8.6}$, in correspondence of which m_V can assume two distinct values, one peaked around 1 GeV and the other for $m_V \lesssim 200$ MeV. The origin of these solutions can be traced back to the peculiar q^2 dependence of Eqs. (3.7), (3.8), which can give rise, for specific choices of m_V , to destructive and/or constructive interference in the DEFT Wilson coefficients that are fitted to the experimental bins. In particular we observe that, while at $m_V \approx 1$ GeV the global fit is dominated by the branching ratio $\text{BR}(B \rightarrow K \mu^+ \mu^-)$, for the region at lower masses the prevalent channel is given by the “angular” P'_5 , which requires the biproduct $\mathcal{C}_4^{bsV} \cdot \mathcal{C}_4^{\mu\mu V}$ to be larger than $\mathcal{C}_4^{bsV} \cdot \tilde{\mathcal{C}}_4^{\mu\mu V}$. Note that the solution with $m_V \approx 1$ GeV is characterised by a non-negligible width, as highlighted by the peak around $\gamma_V \approx 0.4 - 0.5$ in the posterior pdf. This does not seem to be the case instead for $m_V \lesssim 200$ MeV, thus highlighting the prevalence of different observables in the two regions.

The fit results in the case of DEFT operators of dimension 6 in the $b - s$ current and dimension 4 in $\mu - \mu$ are presented in Fig. 1(b) (we dub this as the $6\bar{4}$ model hereafter). The colour scheme is the same as in Fig. 1(a). $\mathcal{C}_6^{bsV} \cdot \mathcal{C}_4^{\mu\mu V}$ is required to be negative in the high-mass region (in red), and positive in the low-mass one (in green). Quantitative differences with respect to the $4\bar{4}$ model can be found in this case, driven by the different q^2 dependence of the NP contributions, but we can also highlight a few qualitative similarities, for example, there remains a strong correlation between m_V and the coupling product $\mathcal{C}_6^{bsV} \cdot \mathcal{C}_4^{\mu\mu V}$ in the high-mass region. However, the high-probability region of the pdf is peaked now at higher m_V . In the low-mass region one can see that $\mathcal{C}_6^{bsV} \cdot \mathcal{C}_4^{\mu\mu V}$ is bound to a narrow range whereas m_V follows a distribution similar to the $4\bar{4}$ model. The region of high probability at $m_V \approx 1$ GeV appears more pronounced in the $6\bar{4}$ model than in the $4\bar{4}$ model, and it seems to require a comparatively smaller width. This is due to the explicit q^2 dependence of the bsV coupling in the $6\bar{4}$ model, which facilitates a good fit to many of the $\text{BR}(B \rightarrow K \mu^+ \mu^-)$ data bins.

Note that a fit performed in the case of DEFT operators of dimension 4 in the $b - s$ current and dimension 6 in $\mu - \mu$ ($4\bar{6}$ model) yields results perfectly analogous to the ones shown in Fig. 1(b), given the equal q^2 dependence of the two scenarios, presented in Eqs. (3.7), (3.8).

⁷Exceptions to this statement apply if one advocates for a very conservative treatment of the hadronic uncertainties or, alternatively, for an additional universal NP component in both the electron and muon vector currents. Indeed, if one allows for either one of these possibilities it becomes easier to accommodate NP contributions to the muon axial current of the same size as the ones in the muon vector current (and hence $|\mathcal{C}_4^{\mu\mu V}| \approx |\tilde{\mathcal{C}}_4^{\mu\mu V}|$) [24, 25, 28, 30, 33, 35, 36].

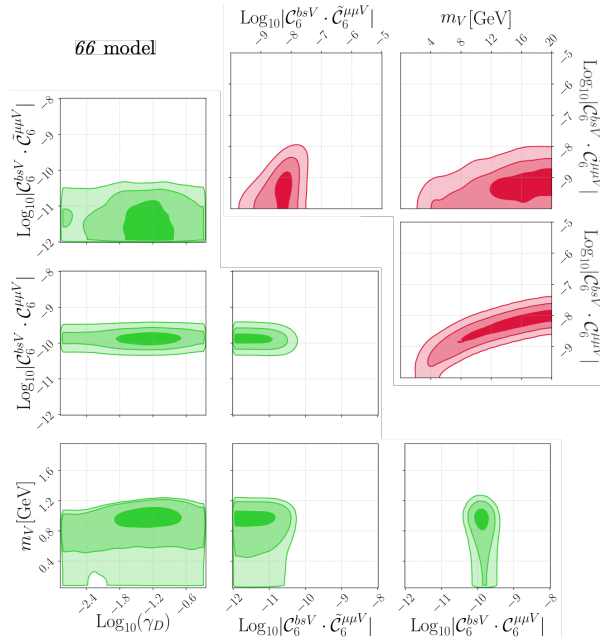
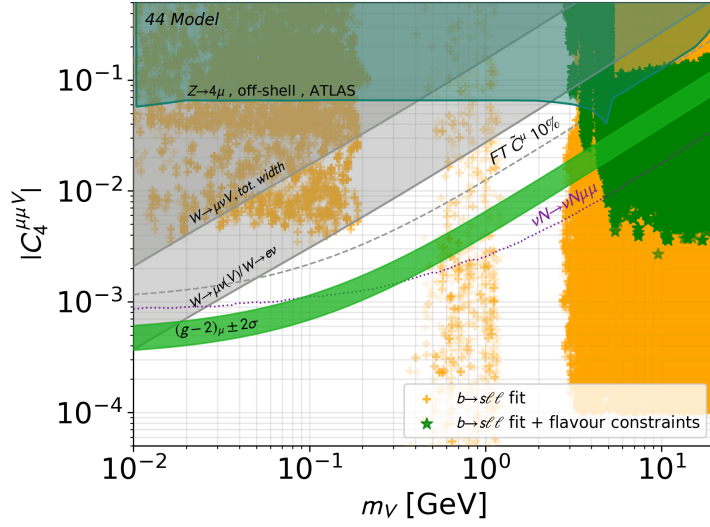


Figure 2: Inference of model parameters from a fit to $b \rightarrow s$ anomalous data with DEFT operators of dimension 6 in both the $b - s$ and $\mu - \mu$ currents (66 model). The colour scheme is the same as in Fig. 1. Note that the couplings C_6^{bsV} , $C_6^{\mu\mu V}$ and $\tilde{C}_6^{\mu\mu V}$ are reported in units of GeV^{-2} .

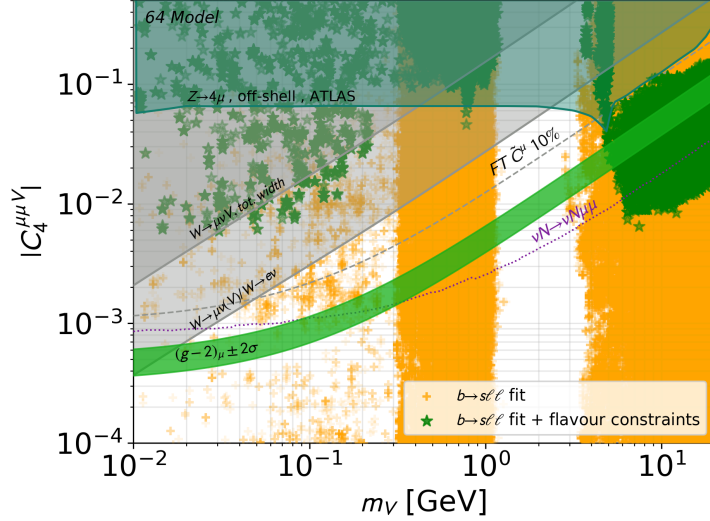
Finally, we present in Fig. 2 the marginalised 2D pdf of the fit in the case of DEFT operators of dimension 6 in both the $b - s$ and $\mu - \mu$ currents (66 model). The colour scheme is the same as in Fig. 1. The fit shows many qualitative similarities to the 64 case, with notable differences pertaining mostly to the favoured values of the couplings, due to the different q^2 dependence, and a pronounced high-probability peak at $m_V \approx 1 \text{ GeV}$, $\gamma_V \approx 10^{-1.8} - 10^{-1}$, with lower probability when the V mass becomes smaller. Note how the transition to the region where the angular observables exert the greatest relative pull, at very low m_V , is much smoother in this model than in the previous cases, indicating that it is not difficult to fit the $\text{BR}(B \rightarrow K\mu^+\mu^-)$ bin data over a broader mass range, due to the additional q^2 -dependence of the muon coupling.

5.2 Including all flavour constraints

We can now apply the constraints introduced in Secs. 4.1, 4.2 to the high-probability regions of the fits described above. We present the results for the 44 model in Fig. 3(a), in the plane of the vector muon coupling versus the FIP mass m_V . The yellow points in the figure are within the 2σ regions of the fits to $b \rightarrow s$ anomalies described in Sec. 5.1. Green points satisfy, additionally, $B_s - \bar{B}_s$ mixing and $B_s \rightarrow \mu\mu$ constraints, as well as ATLAS $Z \rightarrow \mu\mu V^{(*)}$ at the 2σ level, as described in Sec. 4.2. We have also ensured that all of them pass the constraints on invisible final states from the BaBar searches [80, 81], numerically recast as described in Ref. [8], and the bounds from resonant $B \rightarrow K^*\mu^+\mu^-$



(a)



(b)

Figure 3: Constraints on the parameter space consistent with the LFUV anomalies (yellow points) in the plane of $C_4^{\mu\mu V}$ versus the vector mass m_V . (a) The 44 model. (b) The 64 model. Besides being consistent at 2σ with the $b \rightarrow s$ anomalies, all green points satisfy the constraints from $B \rightarrow K + \text{inv.}$, $B \rightarrow K^* \mu\mu$, $B_s - \bar{B}_s$ mixing, $B_s \rightarrow \mu\mu$ and $Z \rightarrow 4\mu$ (off-shell+on-shell) at 2σ , applied following the procedure described in the text. We show overlaid the bounds that do not depend on the hadronic sector and/or on $\Gamma_{V,\text{inv.}}$. The blue region covers the parameter space excluded by the multilepton ATLAS search [67] (off-shell), whereas the grey regions show bounds from LFUV in W -decay (see main text). The green band is consistent with the $(g-2)_\mu$ measurement [37] at 2σ , with no fine tuning of the couplings. All points above the green band require a non-zero $\tilde{C}_4^{\mu\mu V}$, with the dashed grey line indicating a 10% fine tuning with $C_4^{\mu\mu V}$. The dotted purple line in both panels shows the upper bound from neutrino trident production [59], obtained under the assumption that the coupling of V to neutrinos is of the same size as $C_4^{\mu\mu V}$.

at LHCb, also described in Ref. [8]. We finally overlay the remaining limits, which are independent of $\Gamma_{V,\text{inv}}$. The green band corresponds to $\mathcal{C}_4^{\mu\mu V}$ being consistent at 2σ with the $(g-2)_\mu$ measurement [37].

Some of the constraints applied to the parameter space depend explicitly on both $\mathcal{C}_4^{\mu\mu V}$ and $\tilde{\mathcal{C}}_4^{\mu\mu V}$. This is the case, particularly, of the W -decay bound of Eq. (4.8) and forward, and the numerical recast of the $Z \rightarrow 4\mu$ cross-section bound. When these bounds are applied to regions of the parameter space for which $\mathcal{C}_4^{\mu\mu V}$ is too large to yield a value of $\delta(g-2)_\mu$ in agreement with the experimental determination, we tune $\tilde{\mathcal{C}}_4^{\mu\mu V}$ as required to bring $\delta(g-2)_\mu$ down to the measured 2σ region, cf. Sec. 4.3.⁸ The dashed grey line in the figure indicates a fine tuning at the 10% level.

FIPs with mass above the B -meson can easily yield an excellent fit to the experimental data while escaping all current constraints. This conclusion holds for the 44 model, shown in Fig. 3(a), as well as for the 64 model, shown in Fig. 3(b). The favoured parameter space in the 64 model is in agreement with the results obtained in the UV model of Ref. [8]. Incidentally, we find it remarkable that these very compact simplified-model solutions to the $b \rightarrow s$ anomalies feature also excellent prospect to solve the $(g-2)_\mu$ anomaly with no fine tuning required. In the high mass region, the lower limit on the green points distribution arises from the B_s -mixing constraints on \mathcal{C}_4^{bsV} and \mathcal{C}_6^{bsV} and the upper limit from the ATLAS Collaboration [67] search for $Z \rightarrow 4\mu$.

We observe in Fig. 3(b) that for the 64 model the fit yields a large number of points compatible with the various B -physics constraints in the very low-mass region of the parameter space, $m_V \ll 2M_\mu$. On the other hand, the required couplings to the muon are typically quite large, to overcome the strong bounds on $\mathcal{C}_6^{bsV}/\Lambda^2$ from $B \rightarrow K + \text{invisible}$. This leads to $\delta(g-2)_\mu$ exceeding the experimental value and, consequently, a unified solution to all anomalies requires the aforementioned fine tuning of the axial-vector muon coupling against the vector one. The overwhelming majority of these points are excluded by flavour-universality tests in W decays, as measured at the LHC [68].

We show in Fig. 4 the corresponding results for the 66 model. There appear to be extremely few points that can pass all the cuts simultaneously, with the limit from the multilepton ATLAS search [67] dominating the constraints on the muon coupling. This exclusion reflects the fact that the FIP coupling to the muon, $\mathcal{C}_6^{\mu\mu V}$, is of dimension 6 and thus more sensitive to high-energy processes than in the 44 and 64 cases.

We point out, finally, that in the presence of a neutrino coupling, stringent constraints from neutrino trident production apply [59], potentially excluding a common solution for the $(g-2)_\mu$ and LFUV anomalies in the high-mass region. For indicative purposes we show as a dotted purple line in both panels of Fig. 3 the upper bound obtained under the assumption that the coupling of V to neutrinos is of the same size as $\mathcal{C}_4^{\mu\mu V}$. This would be indeed the case for $SU(2)_L$ -conserving interactions of the V with the lepton doublet, like in the well-known $L_\mu - L_\tau$ gauge group. However, it is possible to envision more elaborate UV constructions that could allow one to suppress the coupling to the neutrino

⁸As the sign of $\tilde{\mathcal{C}}_4^{\mu\mu V}$ is not fixed by this procedure, we choose it in agreement with the requirements from the $b \rightarrow s$ fits, i.e., opposite to the sign of $\mathcal{C}_4^{\mu\mu V}$.

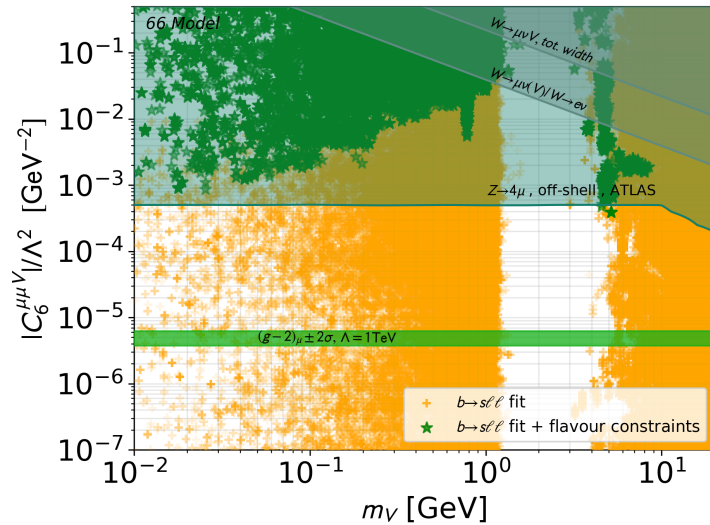


Figure 4: Constraints on the parameter space consistent with the LFUV anomalies (yellow points) in the plane of $C_6^{\mu\mu V}$ versus the vector mass m_V for the 66 model. The colour scheme is the same as in Fig. 3. The position of the $(g-2)_\mu$ 2σ band corresponds to a UV scale $\Lambda = 1$ TeV, see Eq. (4.15).

with respect to the corresponding charged lepton, in which case the purple line in Fig. 3 would shift upwards.⁹ Alternatively, the presence of extra particles and interactions in the UV may introduce contributions to the $(g-2)_\mu$ beyond the ones computed in our bottom-up approach. The green band in Fig. 3 would in that case shift downwards.

6 Summary and conclusions

In this paper we have performed a comprehensive phenomenological analysis of a set of simplified models providing a combined solution to the anomalous magnetic moment of the muon and the flavour anomalies emerged at LHCb in $b \rightarrow sl^+l^-$ transitions (both flavour-conserving and lepton-flavour violating). Our simplified models are based on a set of operators of the Dark EFT, or DEFT, where with this term we encompass a broad range of interactions between the SM and one or more light, feebly interacting particles (FIPs) that find their origin in heavy degrees of freedom integrated out of the theory. The most promising models for fitting both anomalies are based on vector FIPs, with the FIP exchange at low energy giving rise to the anomalies in flavour and $(g-2)_\mu$.

⁹One may construct for instance a 2-Higgs doublet model where the additional Higgs doublet and extra VL heavy leptons all carry $U(1)_D$ charge: $\Theta : (\mathbf{1}, \mathbf{2}, 1/2, Q_D)$, $E : (\mathbf{1}, \mathbf{1}, 1, Q_D)$. Yukawa couplings with the SM left-handed muon doublet, L_μ , of the type $\lambda E \Theta^\dagger L_\mu$, generate a left-chiral coupling $g_L^{\mu\mu}$ of V to the muons once $U(1)_D$ is broken. The coupling to neutrinos is absent at the tree level. Typically one gets $g_L^{\mu\mu} \approx -g_D Q_D \lambda^2 v_D^2 / 2m_E^2$. The spectrum will have to feature additional scalar singlets/multiplets of $SU(2)_L$, whose scalar potential and dark charges have to be adjusted to cancel the direct V/Z mixing and to raise the mass of the charged scalars above direct LHC bounds.

We have divided our simplified models in categories determined by the explicit momentum dependence of the FIP interaction with the $b-s$ and $\mu-\mu$ vector currents. For all categories, after performing a global fit to the experimental data we have applied a large set of constraints to the favoured parameter space, extracted from direct measurements of the $B \rightarrow K + \text{invisible}$ branching ratio, $B \rightarrow K^* \mu^+ \mu^-$ resonant decays, the measurements of $\text{BR}(B_s \rightarrow \mu^+ \mu^-)$, and B_s -mixing. Moreover, we have computed for the first time the strong constraints arising from several precision measurements associated with W - and Z -boson decay, namely the measurement of the $Z \rightarrow 4\mu$ cross section at ATLAS and the decay $W \rightarrow \mu + \text{invisible}$. We find that unified explanations of the $(g-2)_\mu$ and $b \rightarrow sl^+l^-$ anomalies exist and pass all the constraints in a model based on vector-mediator exchange with DEFT operators of dimension 4 in both the $b-s$ and $\mu-\mu$ vector currents (model 44 , with no momentum dependence of the couplings), and in vector-mediator exchange with dimension 6 in the $b-s$ current (q^2 -dependence of the coupling) and dimension 4 in $\mu-\mu$ (we call it model 64). In both models the typical range of the vector mediator mass is $m_V \gtrsim 4 \text{ GeV}$ and the solution to the $(g-2)_\mu$ anomaly does not require any fine tuning of the vector and axial-vector couplings of the V with the muon. Despite a similar mass range for the flavour anomalies in models 44 and 64 , the observables $B_s \rightarrow \mu\mu$ and $R_{\Delta M_s}$ are sensitive to the momentum dependence of their couplings and thus will be able to discriminate between them.

FIPs with $m_V > 20 \text{ GeV}$ are also likely to provide a good fit to the $b \rightarrow sl^+l^-$ anomalies. However, we have worked here under the assumption that the mixing of V with the electroweak sector of the SM can be neglected. As this hypothesis may break down when approaching closely the Z mass from below, possibly leading to additional limits from processes such as $Z \rightarrow \gamma V$ and others, we leave a proper study of the “transitional” regime between light and heavy NP to future work.

While in model 44 the only viable unified solution lies in the $m_V \gtrsim 4 \text{ GeV}$ range, in model 64 the global analysis of $b \rightarrow sl^+l^-$ observables highlights additionally a region of good fit at $m_V \approx 0.01 - 1 \text{ GeV}$ passing all flavour constraints. However, this region of the parameter space is characterised by a large muon coupling and requires large fine tuning of the vector and axial-vector contributions to satisfy the $(g-2)_\mu$ measurement. More importantly, we find that an upper bound on the muon coupling imposed by the $\Gamma(W \rightarrow \mu\nu V)$ measured width entirely excludes this region of the parameter space.

In summary, we have highlighted in this work viable solutions for a combined explanation of the $(g-2)_\mu$ and $b \rightarrow sl^+l^-$ anomalies, based on the simple exchange of a light particle and characterised by a minimal set of assumptions on the heavy UV completion. Our goal is that of providing a self-standing and fairly broad compendium of the low-energy experimental bounds affecting these scenarios. The emerging parameter space regions and coupling strengths can then be used at face value to guide the model-building efforts in the high-energy sector.

Acknowledgments

L.D. has been supported in part by the INFN “Iniziativa Specifica” Theoretical Astroparticle Physics (TAsP-LNF). This project has received funding from the European Union’s

Horizon 2020 research and innovation programme under the Marie Skłodowska-Curie grant agreement No. 101028626. The work of M.F. is supported by the Deutsche Forschungsgemeinschaft (DFG, German Research Foundation) under grant 396021762 - TRR 257, “Particle Physics Phenomenology after the Higgs Discovery”. K.K. is partially supported by the National Science Centre (Poland) under the research Grant No. 2017/26/E/ST2/00470. E.M.S. is supported in part by the National Science Centre (Poland) under the research Grant No. 2017/26/D/ST2/00490.

A B -meson decays in the DEFT basis

This appendix collects the most important ingredients for estimating the FIP contribution to B -meson related observables, as derived directly from the DEFT operators. We eventually compare the results to the standard WET in order to provide a simple dictionary which can be used to re-adapt existing codes to the case of light particles. We use the convention $\sigma_{\mu\nu} = i[\gamma_\mu, \gamma_\nu]/2$ and as customary define B mesons as containing the b quark instead of the antiquark.

A.1 $B \rightarrow K$ process

We start with a simple $B \rightarrow K \ell \bar{\ell}$ process. Following the standard procedure, which relies on factorisation of the full amplitude into a hadronic and a leptonic part, one can express the $\bar{B}(p) \rightarrow \bar{K}(k) \ell(k_1) \bar{\ell}(k_2)$ amplitude as [99]

$$\begin{aligned} \mathcal{M}(\bar{B} \rightarrow \bar{K} \ell \bar{\ell}) &= \frac{i \alpha_{\text{em}}}{4\pi \mathcal{N}} (F_V p^\mu [\bar{\ell} \gamma_\mu \ell] + F_A p^\mu [\bar{\ell} \gamma_\mu \gamma_5 \ell] \\ &\quad + (F_S + \cos \theta F_T) [\bar{\ell} \ell] + (F_P + \cos \theta F_{T5}) [\bar{\ell} \gamma_5 \ell]) , \end{aligned} \quad (\text{A.1})$$

where $\mathcal{N}^{-1} = (4G_F/\sqrt{2}) V_{tb} V_{ts}^*$ and θ is the angle between the B and the exiting lepton ℓ (which is assumed to be a muon in this work) in the B -meson frame. We have furthermore denoted with brackets the contraction of the leptonic current on the vacuum di-muon final state, such as for instance,

$$[\bar{\ell} \gamma_\mu \gamma_5 \ell] \equiv \langle \ell^- \ell^+ | \bar{\ell} \gamma_\mu \gamma_5 \ell | 0 \rangle . \quad (\text{A.2})$$

The coefficients F_V , F_A , F_S , F_P , F_T and F_{T5} are given in Ref. [99] as functions of the Wilson coefficients of the WET basis. The $B \rightarrow K$ matrix elements of the vector current are usually parametrised as [100]

$$\langle \bar{K}(k) | \bar{s} \gamma^\rho b | \bar{B}(p) \rangle = f_+(q^2) \left(-\frac{q^\rho (M_B^2 - M_K^2)}{q^2} + k^\rho + p^\rho \right) + \frac{f_0(q^2) q^\rho (M_B^2 - M_K^2)}{q^2} , \quad (\text{A.3})$$

where $q = p - k$ and $f_0(q^2)$, $f_+(q^2)$ are the form factors. The complete amplitude then follows from contracting the effective vertices corresponding to the DEFT operators of

Eqs. (2.1)-(2.4). One obtains

$$F_V^{\text{DEFT}} = \frac{4\pi\mathcal{N}}{\alpha_{\text{em}}\Pi} \left(\mathcal{C}_4^{\mu\mu V} \mathcal{C}_4^{bsV} + \frac{q^2}{\Lambda^2} \mathcal{C}^{\text{DEFT}} \right) f_+(q^2), \quad (\text{A.4})$$

$$F_A^{\text{DEFT}} = \frac{4\pi\mathcal{N}}{\alpha_{\text{em}}\Pi} \left(\tilde{\mathcal{C}}_4^{\mu\mu V} \mathcal{C}_4^{bsV} + \frac{q^2}{\Lambda^2} \tilde{\mathcal{C}}^{\text{DEFT}} \right) f_+(q^2), \quad (\text{A.5})$$

$$F_P^{\text{DEFT}} = -\frac{4\pi\mathcal{N}M_\mu}{\alpha_{\text{em}}q^2\Pi} \left[\left(\tilde{\mathcal{C}}_4^{\mu\mu V} \mathcal{C}_4^{bsV} - \frac{q^2}{\Lambda^2} \tilde{\mathcal{C}}^{\text{DEFT}} \right) f_+(q^2) (M_B^2 - M_K^2 + q^2) \right. \\ \left. + \tilde{\mathcal{C}}_4^{\mu\mu V} \mathcal{C}_4^{bsV} f_0(q^2) \frac{(M_B^2 - M_K^2)(q^2 - m_V^2)}{m_V^2} \right], \quad (\text{A.6})$$

$$F_S^{\text{DEFT}} = F_T^{\text{DEFT}} = F_{T5}^{\text{DEFT}} = 0, \quad (\text{A.7})$$

where the propagator Π is defined in Eq. (3.4) and we have introduced

$$\mathcal{C}^{\text{DEFT}} \equiv \mathcal{C}_6^{\mu\mu V} \mathcal{C}_4^{bsV} + \mathcal{C}_4^{\mu\mu V} \mathcal{C}_6^{bsV} + \frac{q^2}{\Lambda^2} \mathcal{C}_6^{\mu\mu V} \mathcal{C}_6^{bsV}, \quad (\text{A.8})$$

$$\tilde{\mathcal{C}}^{\text{DEFT}} \equiv \tilde{\mathcal{C}}_6^{\mu\mu V} \mathcal{C}_4^{bsV} + \tilde{\mathcal{C}}_4^{\mu\mu V} \mathcal{C}_6^{bsV} + \frac{q^2}{\Lambda^2} \tilde{\mathcal{C}}_6^{\mu\mu V} \mathcal{C}_6^{bsV}. \quad (\text{A.9})$$

We can now compare Eqs. (A.4)-(A.7) with the corresponding F_i functions expressed in terms of the WET coefficients, shown, e.g., in Ref. [99], to define a dictionary between the DEFT and WET approaches:

$$C_9^\mu \rightarrow \frac{4\pi\mathcal{N}}{\alpha_{\text{em}}\Pi} \left(\mathcal{C}_4^{\mu\mu V} \mathcal{C}_4^{bsV} + \frac{q^2}{\Lambda^2} \mathcal{C}^{\text{DEFT}} \right), \quad (\text{A.10})$$

$$C_{10}^\mu \rightarrow \frac{4\pi\mathcal{N}}{\alpha_{\text{em}}\Pi} \left(\tilde{\mathcal{C}}_4^{\mu\mu V} \mathcal{C}_4^{bsV} + \frac{q^2}{\Lambda^2} \tilde{\mathcal{C}}^{\text{DEFT}} \right), \quad (\text{A.11})$$

$$C_P^\mu + C_P^{\mu'} \rightarrow -\frac{4\pi\mathcal{N}}{\alpha_{\text{em}}\Pi} \frac{2M_\mu(M_b - M_s)}{m_V^2} \left(\tilde{\mathcal{C}}_4^{\mu\mu V} \mathcal{C}_4^{bsV} + \frac{m_V^2}{\Lambda^2} \tilde{\mathcal{C}}^{\text{DEFT}} \right). \quad (\text{A.12})$$

In the end, we obtain the same results as in Eqs. (3.7)-(3.10), although the coefficients C_P^μ and $C_P^{\mu'}$ arise in a combination that cannot be disentangled in the WET framework for this particular process.

A.2 $B \rightarrow K^*$ process

A similar comparison for B decaying into a vector meson is relatively more involved, due to the larger phase space of the final-state hadrons. Our strategy will be to estimate the relevant amplitude in the helicity basis, following the conventions of Ref. [101]. Employing again the factorisation of the amplitude, one can write

$$\mathcal{M}(\bar{B} \rightarrow \bar{K}^* \ell \ell) = a_V^\mu [\bar{\ell} \gamma_\mu \ell] + a_A^\mu [\bar{\ell} \gamma_\mu \gamma_5 \ell] + a_S [\bar{\ell} \ell] + a_P [\bar{\ell} \gamma_5 \ell] \\ + a_{TR}^\mu \frac{i}{\sqrt{q^2}} [\bar{\ell} q^\nu \sigma_{\mu\nu} P_R \ell] + a_{TL}^\mu \frac{i}{\sqrt{q^2}} [\bar{\ell} q^\nu \sigma_{\mu\nu} P_L \ell], \quad (\text{A.13})$$

where a_V^μ , a_A^μ , a_S , a_P , a_{TR}^μ , a_{TL}^μ , are coefficients containing the hadronic part of the amplitude specific to the $B \rightarrow K^* \ell \ell$ process and we have used once more the bracket notation

of Eq. (A.2) to denote the bracket-contracted leptonic currents. Repeating the same procedure as in Appendix A.1 and introducing the helicity amplitudes defined in Ref. [101], one finds

$$H_V^{\text{DEFT}} \equiv \epsilon_\rho^* a_V^\rho = \frac{\mathcal{N}\tilde{V}_{L\lambda}}{\Pi} \left(C_4^{\mu\mu V} C_4^{bsV} + \frac{q^2}{\Lambda^2} C^{\text{DEFT}} \right), \quad (\text{A.14})$$

$$H_A^{\text{DEFT}} \equiv \epsilon_\rho^* a_A^\rho = \frac{\mathcal{N}\tilde{V}_{L\lambda}}{\Pi} \left(\tilde{C}_4^{\mu\mu V} C_4^{bsV} + \frac{q^2}{\Lambda^2} \tilde{C}^{\text{DEFT}} \right), \quad (\text{A.15})$$

$$H_P^{\text{DEFT}} \equiv a_P + \frac{2M_\mu}{q^2} q_\rho a_A^\rho = -\frac{2\mathcal{N}M_\mu(M_s\tilde{S}_L - M_b\tilde{S}_R)}{\Pi} \frac{\tilde{C}_4^{\mu\mu V} C_4^{bsV} (q^2 - m_V^2)}{q^2 m_V^2}, \quad (\text{A.16})$$

where ϵ_ρ^* denotes the helicity of K^* and the form factors in the helicity basis, $\tilde{V}_{L\lambda}$, \tilde{S}_R , \tilde{S}_L , are defined as in Refs. [101–103]:

$$\langle \bar{K}^* | \bar{s} \not{\epsilon}^*(\lambda) P_L b | \bar{B} \rangle = -i M_B \tilde{V}_{L\lambda}, \quad (\text{A.17})$$

$$\langle \bar{K}^* | \bar{s} P_{L(R)} b | \bar{B} \rangle = i M_B \tilde{S}_{L(R)}. \quad (\text{A.18})$$

Finally, one can compare Eqs. (A.14)–(A.16) with the WET results of Ref. [101] to obtain the same correspondence between the WET and DEFT coefficients C_9^μ and C_{10}^μ as in Eqs. (A.10)–(A.11). Interestingly, we are now able to lift the degeneracy between the C_P^μ and $C_P^{\mu'}$, obtaining two additional relations,

$$C_P^\mu \rightarrow -\frac{4\pi\mathcal{N}}{\alpha_{\text{em}}\Pi} \frac{2M_\mu M_b}{m_V^2} \left(\tilde{C}_4^{\mu\mu V} C_4^{bsV} + \frac{m_V^2}{\Lambda^2} \tilde{C}^{\text{DEFT}} \right), \quad (\text{A.19})$$

$$C_P^{\mu'} \rightarrow \frac{4\pi\mathcal{N}}{\alpha_{\text{em}}\Pi} \frac{2M_\mu M_s}{m_V^2} \left(\tilde{C}_4^{\mu\mu V} C_4^{bsV} + \frac{m_V^2}{\Lambda^2} \tilde{C}^{\text{DEFT}} \right). \quad (\text{A.20})$$

A.3 $B_s \rightarrow \mu\mu$ and B_s -mixing processes

For the case of the $B_s \rightarrow \mu\mu$ decay, the kinematics of the process can be derived directly from the matrix elements:

$$\langle 0 | \bar{s} \gamma^\rho \gamma^5 b | \bar{B}_s(p) \rangle = i f_{B_s} p^\rho, \quad (\text{A.21})$$

$$\langle 0 | \bar{s} \gamma^5 b | \bar{B}_s(p) \rangle = -i \frac{M_{B_s}^2}{M_b + M_s} f_{B_s}, \quad (\text{A.22})$$

where f_{B_s} is the decay constant of the B_s meson.

As was pointed out in Sec. 4.1, only the DEFT operators of dimension four contribute to this process, leading to

$$\mathcal{M}(\bar{B}_s \rightarrow \mu\mu) = -\frac{M_\mu f_{B_s}}{\Pi m_V^2} \tilde{C}_4^{\mu\mu V} C_4^{bsV} (M_{B_s}^2 - m_V^2) [\bar{\ell} \gamma_5 \ell]. \quad (\text{A.23})$$

The above can be compared with the SM prediction to obtain the ratio defined in Eq. (4.2). One can then calculate the R_{B_s} ratio as

$$\begin{aligned} R_{B_s} &= \frac{\text{BR}(B_s \rightarrow \mu^+ \mu^-)_{\text{exp.}}}{\text{BR}(B_s \rightarrow \mu^+ \mu^-)_{\text{SM}}} - 1 \\ &= \left| 1 + \frac{4\pi \mathcal{C}_4^{bsV} \tilde{\mathcal{C}}_4^{\mu\mu V} (m_V^2 - M_{B_s}^2)}{C_{10}^{\text{SM}} \Pi \alpha_{\text{em}} m_V^2} \right|^2 - 1, \end{aligned} \quad (\text{A.24})$$

and check using the WET expression [104] that the link between the DEFT and WET operators can be obtained from the $B \rightarrow K$ one, as advertised in the main text. Note that the amplitude is suppressed when the FIP mass m_V nears M_{B_s} . By expanding in the small coupling limit, one then recovers the main text result Eq. (4.3).

For the case of B_s mixing, the relevant four-quark currents correspond directly to the operators of the WET basis with colour indices contracted in pairs (we follow the conventions of Ref. [105]):

$$\mathcal{O}_1 = (\bar{s}\gamma^\mu P_L b) (\bar{s}\gamma^\mu P_L b), \quad (\text{A.25})$$

$$\tilde{\mathcal{O}}_1 = (\bar{s}\gamma^\mu P_R b) (\bar{s}\gamma^\mu P_R b), \quad (\text{A.26})$$

$$\mathcal{O}_2 = (\bar{s}P_L b) (\bar{s}P_L b), \quad (\text{A.27})$$

$$\tilde{\mathcal{O}}_2 = (\bar{s}P_R b) (\bar{s}P_R b), \quad (\text{A.28})$$

$$\mathcal{O}_4 = (\bar{s}P_L b) (\bar{s}P_R b). \quad (\text{A.29})$$

After simplifying the effective vertices, one obtains

$$C_1 \rightarrow -\frac{1}{\Pi} \left((\mathcal{C}_4^{bsV})^2 + \frac{\mathcal{C}_{B_s}^{\text{DEFT}} M_{B_s}^2}{\Lambda^2} \right), \quad (\text{A.30})$$

$$\tilde{C}_1 \rightarrow 0, \quad (\text{A.31})$$

$$C_2 \rightarrow -\frac{M_b^2}{m_V^2 \Pi} \left((\mathcal{C}_4^{bsV})^2 + \frac{\mathcal{C}_{B_s}^{\text{DEFT}} M_{B_s}^2}{\Lambda^2} \right), \quad (\text{A.32})$$

$$\tilde{C}_2 \rightarrow -\frac{M_s^2}{m_V^2 \Pi} \left((\mathcal{C}_4^{bsV})^2 + \frac{\mathcal{C}_{B_s}^{\text{DEFT}} M_{B_s}^2}{\Lambda^2} \right), \quad (\text{A.33})$$

$$C_4 \rightarrow \frac{2M_b M_s}{m_V^2 \Pi} \left((\mathcal{C}_4^{bsV})^2 + \frac{\mathcal{C}_{B_s}^{\text{DEFT}} M_{B_s}^2}{\Lambda^2} \right), \quad (\text{A.34})$$

where we have defined

$$\mathcal{C}_{B_s}^{\text{DEFT}} = \mathcal{C}_4^{bsV} \mathcal{C}_6^{bsV} + \frac{M_{B_s}^2}{\Lambda^2} (\mathcal{C}_6^{bsV})^2. \quad (\text{A.35})$$

Eventually, the B_s -mixing matrix element is computed in terms of bag parameters $B_{B_s}^{(i)}$, relative to each operator \mathcal{O}_i , by estimating the matrix element of each four-quark

operator. We define [105],

$$\langle B_s | \mathcal{O}_1 | \bar{B}_s \rangle = \langle B_s | \tilde{\mathcal{O}}_1 | \bar{B}_s \rangle = \frac{2}{3} f_{B_s}^2 M_{B_s}^2 B_{B_s}^{(1)}, \quad (\text{A.36})$$

$$\langle B_s | \mathcal{O}_2 | \bar{B}_s \rangle = \langle B_s | \tilde{\mathcal{O}}_2 | \bar{B}_s \rangle = -\frac{5}{12} \left(\frac{M_{B_s}}{M_b + M_s} \right)^2 f_{B_s}^2 M_{B_s}^2 B_{B_s}^{(2)}, \quad (\text{A.37})$$

$$\langle B_s | \mathcal{O}_4 | \bar{B}_s \rangle = \frac{1}{2} \left[\left(\frac{M_{B_s}}{M_b + M_s} \right)^2 + \frac{1}{6} \right] f_{B_s}^2 M_{B_s}^2 B_{B_s}^{(4)}. \quad (\text{A.38})$$

We would like to stress that, compared to the standard WET approach, the bag parameters should not be run from a high scale since the amplitude of the process is estimated directly at the B_s scale. Note also that the DEFT coefficients used in our results do not run, as the currents charged under colour are (axial)-vector.

The experimental observable of interest is the ratio $R_{\Delta M_s}$ between the SM-predicted and NP contribution to the mass difference of the neutral B_s mesons [68]:

$$R_{\Delta M_s} = \left| 1 + \sum_{i=1}^2 R_i \frac{C_i + \tilde{C}_i}{C_1^{\text{SM}}(\mu_b)} + R_4 \frac{C_4}{C_1^{\text{SM}}(\mu_b)} \right| - 1, \quad (\text{A.39})$$

where we have defined the ratios of bag parameters at the b scale by

$$R_i \equiv \frac{\langle B_s | \mathcal{O}_i(\mu_b) | \bar{B}_s \rangle}{\langle B_s | \mathcal{O}_1(\mu_b) | \bar{B}_s \rangle}. \quad (\text{A.40})$$

In the small coupling approximation, one finally finds

$$R_{\Delta M_s} \simeq -\frac{(C_4^{bsV})^2}{C_1^{\text{SM}}(\mu_b) m_V^2} \frac{(M_{B_s}^2 - m_V^2)(m_V^2 + R_2 M_b^2)}{(m_V^2 - M_{B_s}^2)^2 + M_{B_s}^2 \Gamma_V^2}, \quad (\text{A.41})$$

and

$$R_{\Delta M_s} \simeq -\frac{M_{B_s}^2 (C_6^{bsV})^2}{\Lambda^4 C_1^{\text{SM}}(\mu_b)} \frac{(M_{B_s}^2 - m_V^2)(M_{B_s}^2 + R_2 M_b^2)}{(m_V^2 - M_{B_s}^2)^2 + M_{B_s}^2 \Gamma_V^2}. \quad (\text{A.42})$$

References

- [1] A. Datta, J. Liao, and D. Marfatia, *A light Z' for the R_K puzzle and nonstandard neutrino interactions*, Phys. Lett. **B768** (2017) 265–269, [[arXiv:1702.01099](#)].
- [2] F. Sala and D. M. Straub, *A New Light Particle in B Decays?*, Phys. Lett. **B774** (2017) 205–209, [[arXiv:1704.06188](#)].
- [3] A. Datta, J. Kumar, J. Liao, and D. Marfatia, *New light mediators for the R_K and R_{K^*} puzzles*, Phys. Rev. **D97** (2018), no. 11 115038, [[arXiv:1705.08423](#)].
- [4] A. K. Alok, B. Bhattacharya, A. Datta, D. Kumar, J. Kumar, and D. London, *New Physics in $b \rightarrow s\mu^+\mu^-$ after the Measurement of R_{K^*}* , Phys. Rev. **D96** (2017), no. 9 095009, [[arXiv:1704.07397](#)].

- [5] W. Altmannshofer, M. J. Baker, S. Gori, R. Harnik, M. Pospelov, E. Stamou, and A. Thamm, *Light resonances and the low- q^2 bin of R_{K^*}* , JHEP **03** (2018) 188, [[arXiv:1711.07494](#)].
- [6] A. Datta, B. Dutta, S. Liao, D. Marfatia, and L. E. Strigari, *Neutrino scattering and B anomalies from hidden sector portals*, JHEP **01** (2019) 091, [[arXiv:1808.02611](#)].
- [7] A. Datta, J. L. Feng, S. Kamali, and J. Kumar, *Resolving the $(g-2)_\mu$ and B Anomalies with Leptoquarks and a Dark Higgs Boson*, Phys. Rev. **D101** (2020), no. 3 035010, [[arXiv:1908.08625](#)].
- [8] L. Darmé, M. Fedele, K. Kowalska, and E. M. Sessolo, *Flavour anomalies from a split dark sector*, JHEP **08** (2020) 148, [[arXiv:2002.11150](#)].
- [9] **LHCb** Collaboration, R. Aaij et al., *Test of lepton universality in beauty-quark decays*, [arXiv:2103.11769](#).
- [10] **LHCb** Collaboration, R. Aaij et al., *Test of lepton universality with $B^0 \rightarrow K^{*0} \ell^+ \ell^-$ decays*, JHEP **08** (2017) 055, [[arXiv:1705.05802](#)].
- [11] **Belle** Collaboration, A. Abdesselam et al., *Test of Lepton-Flavor Universality in $B \rightarrow K^* \ell^+ \ell^-$ Decays at Belle*, Phys. Rev. Lett. **126** (2021), no. 16 161801, [[arXiv:1904.02440](#)].
- [12] **LHCb** Collaboration, R. Aaij et al., *Differential branching fractions and isospin asymmetries of $B \rightarrow K^{(*)} \mu^+ \mu^-$ decays*, JHEP **06** (2014) 133, [[arXiv:1403.8044](#)].
- [13] **LHCb** Collaboration, R. Aaij et al., *Angular analysis of the $B^0 \rightarrow K^{*0} e^+ e^-$ decay in the low- q^2 region*, JHEP **04** (2015) 064, [[arXiv:1501.03038](#)].
- [14] **LHCb** Collaboration, R. Aaij et al., *Angular analysis and differential branching fraction of the decay $B_s^0 \rightarrow \phi \mu^+ \mu^-$* , JHEP **09** (2015) 179, [[arXiv:1506.08777](#)].
- [15] **CMS** Collaboration, V. Khachatryan et al., *Angular analysis of the decay $B^0 \rightarrow K^{*0} \mu^+ \mu^-$ from pp collisions at $\sqrt{s} = 8$ TeV*, Phys. Lett. B **753** (2016) 424–448, [[arXiv:1507.08126](#)].
- [16] **LHCb** Collaboration, R. Aaij et al., *Angular analysis of the $B^0 \rightarrow K^{*0} \mu^+ \mu^-$ decay using 3 fb^{-1} of integrated luminosity*, JHEP **02** (2016) 104, [[arXiv:1512.04442](#)].
- [17] **LHCb** Collaboration, R. Aaij et al., *Measurements of the S -wave fraction in $B^0 \rightarrow K^+ \pi^- \mu^+ \mu^-$ decays and the $B^0 \rightarrow K^*(892)^0 \mu^+ \mu^-$ differential branching fraction*, JHEP **11** (2016) 047, [[arXiv:1606.04731](#)]. [Erratum: JHEP04,142(2017)].
- [18] **Belle** Collaboration, S. Wehle et al., *Lepton-Flavor-Dependent Angular Analysis of $B \rightarrow K^* \ell^+ \ell^-$* , Phys. Rev. Lett. **118** (2017), no. 11 111801, [[arXiv:1612.05014](#)].
- [19] **CMS** Collaboration, A. M. Sirunyan et al., *Measurement of angular parameters from the decay $B^0 \rightarrow K^{*0} \mu^+ \mu^-$ in proton-proton collisions at $\sqrt{s} = 8$ TeV*, Phys. Lett. B **781** (2018) 517–541, [[arXiv:1710.02846](#)].
- [20] **ATLAS** Collaboration, M. Aaboud et al., *Angular analysis of $B_d^0 \rightarrow K^* \mu^+ \mu^-$ decays in pp collisions at $\sqrt{s} = 8$ TeV with the ATLAS detector*, JHEP **10** (2018) 047, [[arXiv:1805.04000](#)].
- [21] **LHCb** Collaboration, R. Aaij et al., *Measurement of CP -Averaged Observables in the $B^0 \rightarrow K^{*0} \mu^+ \mu^-$ Decay*, Phys. Rev. Lett. **125** (2020), no. 1 011802, [[arXiv:2003.04831](#)].
- [22] **LHCb** Collaboration, R. Aaij et al., *Angular analysis of the $B^+ \rightarrow K^{*+} \mu^+ \mu^-$ decay*, Phys. Rev. Lett. **126** (2021), no. 16 161802, [[arXiv:2012.13241](#)].

- [23] G. D’Amico, M. Nardecchia, P. Panci, F. Sannino, A. Strumia, R. Torre, and A. Urbano, *Flavour anomalies after the R_{K^*} measurement*, JHEP **09** (2017) 010, [[arXiv:1704.05438](#)].
- [24] M. Ciuchini, A. M. Coutinho, M. Fedele, E. Franco, A. Paul, L. Silvestrini, and M. Valli, *New Physics in $b \rightarrow s\ell^+\ell^-$ confronts new data on Lepton Universality*, Eur. Phys. J. **C79** (2019), no. 8 719, [[arXiv:1903.09632](#)].
- [25] M. Algueró, B. Capdevila, A. Crivellin, S. Descotes-Genon, P. Masjuan, J. Matias, and J. Virto, *Emerging patterns of New Physics with and without Lepton Flavour Universal contributions*, Eur. Phys. J. **C79** (2019), no. 8 714, [[arXiv:1903.09578](#)].
- [26] A. K. Alok, A. Dighe, S. Gangal, and D. Kumar, *Continuing search for new physics in $b \rightarrow s\mu\mu$ decays: two operators at a time*, JHEP **06** (2019) 089, [[arXiv:1903.09617](#)].
- [27] A. Datta, J. Kumar, and D. London, *The B anomalies and new physics in $b \rightarrow se^+e^-$* , Phys. Lett. **B797** (2019) 134858, [[arXiv:1903.10086](#)].
- [28] J. Aebischer, W. Altmannshofer, D. Guadagnoli, M. Reboud, P. Stangl, and D. M. Straub, *B -decay discrepancies after Moriond 2019*, Eur. Phys. J. C **80** (2020), no. 3 252, [[arXiv:1903.10434](#)].
- [29] K. Kowalska, D. Kumar, and E. M. Sessolo, *Implications for new physics in $b \rightarrow s\mu\mu$ transitions after recent measurements by Belle and LHCb*, Eur. Phys. J. **C79** (2019), no. 10 840, [[arXiv:1903.10932](#)].
- [30] M. Ciuchini, M. Fedele, E. Franco, A. Paul, L. Silvestrini, and M. Valli, *Lessons from the $B^{0,+} \rightarrow K^{*0,+}\mu^+\mu^-$ angular analyses*, Phys. Rev. D **103** (2021), no. 1 015030, [[arXiv:2011.01212](#)].
- [31] T. Hurth, F. Mahmoudi, and S. Neshatpour, *Model independent analysis of the angular observables in $B^0 \rightarrow K^{*0}\mu^+\mu^-$ and $B^+ \rightarrow K^{*+}\mu^+\mu^-$* , Phys. Rev. D **103** (2021) 095020, [[arXiv:2012.12207](#)].
- [32] J. Alda, J. Guasch, and S. Peñaranda, *Anomalies in B mesons decays: a phenomenological approach*, Eur. Phys. J. Plus **137** (2022), no. 2 217, [[arXiv:2012.14799](#)].
- [33] W. Altmannshofer and P. Stangl, *New physics in rare B decays after Moriond 2021*, Eur. Phys. J. C **81** (2021), no. 10 952, [[arXiv:2103.13370](#)].
- [34] L.-S. Geng, B. Grinstein, S. Jäger, S.-Y. Li, J. Martin Camalich, and R.-X. Shi, *Implications of new evidence for lepton-universality violation in $b \rightarrow s\ell^+\ell^-$ decays*, Phys. Rev. D **104** (2021), no. 3 035029, [[arXiv:2103.12738](#)].
- [35] M. Algueró, B. Capdevila, S. Descotes-Genon, J. Matias, and M. Novoa-Brunet, *$b \rightarrow s\ell\ell$ global fits after Moriond 2021 results*, in 55th Rencontres de Moriond on QCD and High Energy Interactions, 4, 2021. [[arXiv:2104.08921](#)].
- [36] M. Ciuchini, M. Fedele, E. Franco, A. Paul, L. Silvestrini, and M. Valli, *New Physics without bias: Charming Penguins and Lepton Universality Violation in $b \rightarrow s\ell^+\ell^-$ decays*, [[arXiv:2110.10126](#)].
- [37] **Muon $g - 2$ Collaboration**, B. Abi et al., *Measurement of the positive muon anomalous magnetic moment to 0.46 ppm*, Phys. Rev. Lett. **126** (Apr, 2021) 141801.
- [38] M. Davier, A. Hoecker, B. Malaescu, and Z. Zhang, *Reevaluation of the hadronic vacuum polarisation contributions to the Standard Model predictions of the muon $g - 2$ and $\alpha(m_Z^2)$*

- using newest hadronic cross-section data, Eur. Phys. J. C **77** (2017), no. 12 827, [[arXiv:1706.09436](#)].
- [39] A. Keshavarzi, D. Nomura, and T. Teubner, *Muon $g - 2$ and $\alpha(M_Z^2)$: a new data-based analysis*, Phys. Rev. D **97** (2018), no. 11 114025, [[arXiv:1802.02995](#)].
- [40] G. Colangelo, M. Hoferichter, and P. Stoffer, *Two-pion contribution to hadronic vacuum polarization*, JHEP **02** (2019) 006, [[arXiv:1810.00007](#)].
- [41] M. Hoferichter, B.-L. Hoid, and B. Kubis, *Three-pion contribution to hadronic vacuum polarization*, JHEP **08** (2019) 137, [[arXiv:1907.01556](#)].
- [42] M. Davier, A. Hoecker, B. Malaescu, and Z. Zhang, *A new evaluation of the hadronic vacuum polarisation contributions to the muon anomalous magnetic moment and to $\alpha(m_Z^2)$* , Eur. Phys. J. C **80** (2020), no. 3 241, [[arXiv:1908.00921](#)]. [Erratum: Eur.Phys.J.C **80**, 410 (2020)].
- [43] A. Keshavarzi, D. Nomura, and T. Teubner, *$g - 2$ of charged leptons, $\alpha(M_Z^2)$, and the hyperfine splitting of muonium*, Phys. Rev. D **101** (2020), no. 1 014029, [[arXiv:1911.00367](#)].
- [44] A. Kurz, T. Liu, P. Marquard, and M. Steinhauser, *Hadronic contribution to the muon anomalous magnetic moment to next-to-next-to-leading order*, Phys. Lett. B **734** (2014) 144–147, [[arXiv:1403.6400](#)].
- [45] K. Melnikov and A. Vainshtein, *Hadronic light-by-light scattering contribution to the muon anomalous magnetic moment revisited*, Phys. Rev. D **70** (2004) 113006, [[hep-ph/0312226](#)].
- [46] P. Masjuan and P. Sanchez-Puertas, *Pseudoscalar-pole contribution to the $(g_\mu - 2)$: a rational approach*, Phys. Rev. D **95** (2017), no. 5 054026, [[arXiv:1701.05829](#)].
- [47] G. Colangelo, M. Hoferichter, M. Procura, and P. Stoffer, *Dispersion relation for hadronic light-by-light scattering: two-pion contributions*, JHEP **04** (2017) 161, [[arXiv:1702.07347](#)].
- [48] M. Hoferichter, B.-L. Hoid, B. Kubis, S. Leupold, and S. P. Schneider, *Dispersion relation for hadronic light-by-light scattering: pion pole*, JHEP **10** (2018) 141, [[arXiv:1808.04823](#)].
- [49] A. Gérardin, H. B. Meyer, and A. Nyffeler, *Lattice calculation of the pion transition form factor with $N_f = 2 + 1$ Wilson quarks*, Phys. Rev. D **100** (2019), no. 3 034520, [[arXiv:1903.09471](#)].
- [50] J. Bijnens, N. Hermansson-Truedsson, and A. Rodríguez-Sánchez, *Short-distance constraints for the HLbL contribution to the muon anomalous magnetic moment*, Phys. Lett. B **798** (2019) 134994, [[arXiv:1908.03331](#)].
- [51] G. Colangelo, F. Hagelstein, M. Hoferichter, L. Laub, and P. Stoffer, *Longitudinal short-distance constraints for the hadronic light-by-light contribution to $(g - 2)_\mu$ with large- N_c Regge models*, JHEP **03** (2020) 101, [[arXiv:1910.13432](#)].
- [52] G. Colangelo, M. Hoferichter, A. Nyffeler, M. Passera, and P. Stoffer, *Remarks on higher-order hadronic corrections to the muon $g-2$* , Phys. Lett. B **735** (2014) 90–91, [[arXiv:1403.7512](#)].
- [53] T. Blum, N. Christ, M. Hayakawa, T. Izubuchi, L. Jin, C. Jung, and C. Lehner, *Hadronic Light-by-Light Scattering Contribution to the Muon Anomalous Magnetic Moment from Lattice QCD*, Phys. Rev. Lett. **124** (2020), no. 13 132002, [[arXiv:1911.08123](#)].

- [54] T. Aoyama, M. Hayakawa, T. Kinoshita, and M. Nio, *Complete Tenth-Order QED Contribution to the Muon $g-2$* , Phys. Rev. Lett. **109** (2012) 111808, [[arXiv:1205.5370](#)].
- [55] T. Aoyama, T. Kinoshita, and M. Nio, *Theory of the anomalous magnetic moment of the electron*, Atoms **7** (2019), no. 1.
- [56] A. Czarnecki, W. J. Marciano, and A. Vainshtein, *Refinements in electroweak contributions to the muon anomalous magnetic moment*, Phys. Rev. D **67** (2003) 073006, [[hep-ph/0212229](#)]. [Erratum: Phys.Rev.D **73**, 119901 (2006)].
- [57] C. Gnendiger, D. Stöckinger, and H. Stöckinger-Kim, *The electroweak contributions to $(g-2)_\mu$ after the Higgs boson mass measurement*, Phys. Rev. D **88** (2013) 053005, [[arXiv:1306.5546](#)].
- [58] **Muon $g-2$ Collaboration**, G. W. Bennett et al., *Final Report of the Muon E821 Anomalous Magnetic Moment Measurement at BNL*, Phys. Rev. **D73** (2006) 072003, [[hep-ex/0602035](#)].
- [59] W. Altmannshofer, S. Gori, M. Pospelov, and I. Yavin, *Neutrino Trident Production: A Powerful Probe of New Physics with Neutrino Beams*, Phys. Rev. Lett. **113** (2014) 091801, [[arXiv:1406.2332](#)].
- [60] W. Altmannshofer, P. Stangl, and D. M. Straub, *Interpreting Hints for Lepton Flavor Universality Violation*, Phys. Rev. **D96** (2017), no. 5 055008, [[arXiv:1704.05435](#)].
- [61] C. Arina, J. Hajer, and P. Klose, *Portal Effective Theories. A framework for the model independent description of light hidden sector interactions*, JHEP **09** (2021) 063, [[arXiv:2105.06477](#)].
- [62] P. J. Fox, R. Harnik, J. Kopp, and Y. Tsai, *LEP Shines Light on Dark Matter*, Phys. Rev. D **84** (2011) 014028, [[arXiv:1103.0240](#)].
- [63] M. Duch, B. Grzadkowski, and J. Wudka, *Classification of effective operators for interactions between the Standard Model and dark matter*, JHEP **05** (2015) 116, [[arXiv:1412.0520](#)].
- [64] F. Bishara, J. Brod, B. Grinstein, and J. Zupan, *Chiral Effective Theory of Dark Matter Direct Detection*, JCAP **02** (2017) 009, [[arXiv:1611.00368](#)].
- [65] A. De Simone and T. Jacques, *Simplified models vs. effective field theory approaches in dark matter searches*, Eur. Phys. J. C **76** (2016), no. 7 367, [[arXiv:1603.08002](#)].
- [66] L. Darmé, S. A. R. Ellis, and T. You, *Light Dark Sectors through the Fermion Portal*, JHEP **07** (2020) 053, [[arXiv:2001.01490](#)].
- [67] **ATLAS Collaboration**, G. Aad et al., *Measurements of differential cross-sections in four-lepton events in 13 TeV proton-proton collisions with the ATLAS detector*, JHEP **07** (2021) 005, [[arXiv:2103.01918](#)].
- [68] **Particle Data Group Collaboration**, P. A. Zyla et al., *Review of Particle Physics*, PTEP **2020** (2020), no. 8 083C01.
- [69] P. J. Fox, I. Low, and Y. Zhang, *Top-philic Z' forces at the LHC*, JHEP **03** (2018) 074, [[arXiv:1801.03505](#)].
- [70] P. Arnan, A. Crivellin, M. Fedele, and F. Mescia, *Generic loop effects of new scalars and fermions in $b \rightarrow s\ell^+\ell^-$ and a vector-like 4th generation*, JHEP **06** (2019) 118, [[arXiv:1904.05890](#)].

- [71] J. Gracey, *Three loop \overline{MS} tensor current anomalous dimension in QCD*, Phys. Lett. B **488** (2000) 175–181, [[hep-ph/0007171](#)].
- [72] J. A. Dror, R. Lasenby, and M. Pospelov, *Dark forces coupled to nonconserved currents*, Phys. Rev. D **96** (2017), no. 7 075036, [[arXiv:1707.01503](#)].
- [73] J. A. Dror, R. Lasenby, and M. Pospelov, *New constraints on light vectors coupled to anomalous currents*, Phys. Rev. Lett. **119** (2017), no. 14 141803, [[arXiv:1705.06726](#)].
- [74] L. Michaels and F. Yu, *Probing new $U(1)$ gauge symmetries via exotic $Z \rightarrow Z'\gamma$ decays*, JHEP **03** (2021) 120, [[arXiv:2010.00021](#)].
- [75] **ATLAS** Collaboration, *Combination of the ATLAS, CMS and LHCb results on the $B_{(s)}^0 \rightarrow \mu^+\mu^-$ decays.*, tech. rep., CERN, Geneva, Aug, 2020. All figures including auxiliary figures are available at <https://atlas.web.cern.ch/Atlas/GROUPS/PHYSICS/CONFNOTES/ATLAS-CONF-2020-049>.
- [76] M. Beneke, C. Bobeth, and R. Szafron, *Power-enhanced leading-logarithmic QED corrections to $B_q \rightarrow \mu^+\mu^-$* , JHEP **10** (2019) 232, [[arXiv:1908.07011](#)].
- [77] C. Bobeth, T. Ewerth, F. Kruger, and J. Urban, *Analysis of neutral Higgs boson contributions to the decays $\bar{B}(s) \rightarrow \ell^+\ell^-$ and $\bar{B} \rightarrow K\ell^+\ell^-$* , Phys. Rev. D **64** (2001) 074014, [[hep-ph/0104284](#)].
- [78] **Flavour Lattice Averaging Group** Collaboration, S. Aoki et al., *FLAG Review 2019: Flavour Lattice Averaging Group (FLAG)*, Eur. Phys. J. C **80** (2020), no. 2 113, [[arXiv:1902.08191](#)].
- [79] **LHCb** Collaboration, R. Aaij et al., *Search for hidden-sector bosons in $B^0 \rightarrow K^{*0}\mu^+\mu^-$ decays*, Phys. Rev. Lett. **115** (2015), no. 16 161802, [[arXiv:1508.04094](#)].
- [80] **BaBar** Collaboration, P. del Amo Sanchez et al., *Search for the Rare Decay $B \rightarrow K\nu\bar{\nu}$* , Phys. Rev. D **82** (2010) 112002, [[arXiv:1009.1529](#)].
- [81] **BaBar** Collaboration, J. P. Lees et al., *Search for $B \rightarrow K^{(*)}\nu\bar{\nu}$ and invisible quarkonium decays*, Phys. Rev. D **87** (2013), no. 11 112005, [[arXiv:1303.7465](#)].
- [82] **Belle-II** Collaboration, F. Abudinén et al., *Search for $B^+ \rightarrow K^+\nu\nu^-$ Decays Using an Inclusive Tagging Method at Belle II*, Phys. Rev. Lett. **127** (2021), no. 18 181802, [[arXiv:2104.12624](#)].
- [83] N. D. Christensen, P. de Aquino, C. Degrande, C. Duhr, B. Fuks, M. Herquet, F. Maltoni, and S. Schumann, *A Comprehensive approach to new physics simulations*, Eur. Phys. J. C **71** (2011) 1541, [[arXiv:0906.2474](#)].
- [84] C. Degrande, C. Duhr, B. Fuks, D. Grellscheid, O. Mattelaer, and T. Reiter, *UFO - The Universal FeynRules Output*, Comput. Phys. Commun. **183** (2012) 1201–1214, [[arXiv:1108.2040](#)].
- [85] A. Alloul, N. D. Christensen, C. Degrande, C. Duhr, and B. Fuks, *FeynRules 2.0 - A complete toolbox for tree-level phenomenology*, Comput. Phys. Commun. **185** (2014) 2250–2300, [[arXiv:1310.1921](#)].
- [86] J. Alwall, R. Frederix, S. Frixione, V. Hirschi, F. Maltoni, O. Mattelaer, H. S. Shao, T. Stelzer, P. Torrielli, and M. Zaro, *The automated computation of tree-level and next-to-leading order differential cross sections, and their matching to parton shower simulations*, JHEP **07** (2014) 079, [[arXiv:1405.0301](#)].

- [87] **CMS** Collaboration, A. M. Sirunyan et al., *Search for an $L_\mu - L_\tau$ gauge boson using $Z \rightarrow 4\mu$ events in proton-proton collisions at $\sqrt{s} = 13$ TeV*, Phys. Lett. B **792** (2019) 345–368, [[arXiv:1808.03684](#)].
- [88] F. Bishara, U. Haisch, and P. F. Monni, *Regarding light resonance interpretations of the B decay anomalies*, Phys. Rev. **D96** (2017), no. 5 055002, [[arXiv:1705.03465](#)].
- [89] S. G. Karshenboim, D. McKeen, and M. Pospelov, *Constraints on muon-specific dark forces*, Phys. Rev. D **90** (2014), no. 7 073004, [[arXiv:1401.6154](#)]. [Addendum: Phys.Rev.D **90**, 079905 (2014)].
- [90] **BaBar** Collaboration, J. P. Lees et al., *Search for a muonic dark force at BABAR*, Phys. Rev. D **94** (2016), no. 1 011102, [[arXiv:1606.03501](#)].
- [91] **Belle-II** Collaboration, I. Adachi et al., *Search for an Invisibly Decaying Z' Boson at Belle II in $e^+e^- \rightarrow \mu^+\mu^-(e^\pm\mu^\mp)$ Plus Missing Energy Final States*, Phys. Rev. Lett. **124** (2020), no. 14 141801, [[arXiv:1912.11276](#)].
- [92] B. Holdom, *Two $U(1)$'s and Epsilon Charge Shifts*, Phys. Lett. B **166** (1986) 196–198.
- [93] **LHCb** Collaboration, R. Aaij et al., *Measurement of the $B^0 \rightarrow K^{*0}e^+e^-$ branching fraction at low dilepton mass*, JHEP **05** (2013) 159, [[arXiv:1304.3035](#)].
- [94] J. Beacham et al., *Physics Beyond Colliders at CERN: Beyond the Standard Model Working Group Report*, J. Phys. **G47** (2020), no. 1 010501, [[arXiv:1901.09966](#)].
- [95] F. Jegerlehner and A. Nyffeler, *The Muon $g-2$* , Phys. Rept. **477** (2009) 1–110, [[arXiv:0902.3360](#)].
- [96] F. S. Queiroz and W. Shepherd, *New Physics Contributions to the Muon Anomalous Magnetic Moment: A Numerical Code*, Phys. Rev. **D89** (2014), no. 9 095024, [[arXiv:1403.2309](#)].
- [97] J. De Blas et al., *HEPfit: a code for the combination of indirect and direct constraints on high energy physics models*, Eur. Phys. J. C **80** (2020), no. 5 456, [[arXiv:1910.14012](#)].
- [98] A. Caldwell, D. Kollar, and K. Kroninger, *BAT: The Bayesian Analysis Toolkit*, Comput. Phys. Commun. **180** (2009) 2197–2209, [[arXiv:0808.2552](#)].
- [99] C. Bobeth, G. Hiller, and G. Piranishvili, *Angular distributions of $\bar{B} \rightarrow \bar{K}\ell^+\ell^-$ decays*, JHEP **12** (2007) 040, [[arXiv:0709.4174](#)].
- [100] J. A. Bailey et al., *$B \rightarrow Kl^+l^-$ Decay Form Factors from Three-Flavor Lattice QCD*, Phys. Rev. D **93** (2016), no. 2 025026, [[arXiv:1509.06235](#)].
- [101] S. Jäger and J. Martin Camalich, *On $B \rightarrow V\ell\ell$ at small dilepton invariant mass, power corrections, and new physics*, JHEP **05** (2013) 043, [[arXiv:1212.2263](#)].
- [102] A. Bharucha, D. M. Straub, and R. Zwicky, *$B \rightarrow V\ell^+\ell^-$ in the Standard Model from light-cone sum rules*, JHEP **08** (2016) 098, [[arXiv:1503.05534](#)].
- [103] R. R. Horgan, Z. Liu, S. Meinel, and M. Wingate, *Rare B decays using lattice QCD form factors*, PoS LATTICE2014 (2015) 372, [[arXiv:1501.00367](#)].
- [104] M. Beneke, C. Bobeth, and R. Szafron, *Enhanced electromagnetic correction to the rare B -meson decay $B_{s,d} \rightarrow \mu^+\mu^-$* , Phys. Rev. Lett. **120** (2018), no. 1 011801, [[arXiv:1708.09152](#)].

- [105] **Fermilab Lattice, MILC** Collaboration, A. Bazavov et al., $B_{(s)}^0$ -mixing matrix elements from lattice QCD for the Standard Model and beyond, Phys. Rev. D **93** (2016), no. 11 113016, [[arXiv:1602.03560](https://arxiv.org/abs/1602.03560)].